atmosphere

MDPI

Article

Analysis of the COVID-19 Influence on Air Quality in Urban Areas of Japan Using Multiple Satellites and Ground-Based Measurements

Tamaki Fujinawa [1,*], Satoshi Inomata [1], Takafumi Sugita [1], Kohei Ikeda [1], Masahiro Yamaguchi [2] and Hiroshi Tanimoto [1]

[1] Earth System Division, National Institute for Environmental Studies, Tsukuba 305-8506, Japan; ino@nies.go.jp (S.I.); tsugita@nies.go.jp (T.S.); ikeda.kohei@nies.go.jp (K.I.); tanimoto@nies.go.jp (H.T.)
[2] Research Institute for Global Change, Japan Agency for Marine-Earth Science and Technology, Yokohama 236-0001, Japan; myamaguchi@jamstec.go.jp
* Correspondence: fujinawa.tamaki@nies.go.jp; Tel.: +81-29-850-2567

Abstract

We examined the effect of the coronavirus disease 2019 (COVID-19) pandemic on air quality in the Kanto region of Japan using multiple satellites and ground-based observations. The vertical column density (VCD) of nitrogen dioxide (NO_2) derived from the Ozone Monitoring Instrument (OMI) and the Tropospheric Monitoring Instrument (TROPOMI) showed decreases of 38% and 27%, on average, respectively, in March of 2020, compared with the same month in 2015–2019, for OMI and in 2019 for TROPOMI. Surface NO_2 concentrations measured by the Atmospheric Environmental Regional Observation System (AEROS) also declined by up to 22% relative to the 2015–2019 mean, which is consistent with previously reported reductions. To investigate interactions between ozone (O_3) and NO_x, we calculated the ratio of non-methane hydrocarbon (NMHC) and NO_x and potential ozone (PO) surface concentrations from the AEROS data. The results indicated that the ozone formation regime in the Kanto region remained within the NMHC-limited domain during the COVID-19 period and was unchanged from the previous five years. Nevertheless, the baseline O_3 concentration decreased by 2.5–8.5 ppbv, depending on site (urban vs. suburban) and year (2020 vs. 2021). Diurnal variations in PO concentrations (defined as O_3 + NO_2-0.1NO_x), which is the net O_3 concentration produced by photochemical reactions and/or transport excluding the NO titration effect, showed significant reductions of 6.3 ppbv in 2020 and 3.2 ppbv in 2021, suggesting that lower PO levels were mainly attributed to the reductions in baseline O_3 concentrations in 2020. These findings highlight how pandemic-related emission reductions affected chemical processes and dynamics related to both NO_x and O_3 in a major Japanese metropolitan region.

Keywords: remote sensing; satellite; ground-based measurements; air pollution; COVID-19; nitrogen dioxide

Academic Editor: Kai-Jen Chuang

Received: 5 April 2026
Revised: 1 May 2026
Accepted: 2 May 2026
Published: 11 May 2026

1. Introduction

Nitrogen oxides (NO_x = NO + NO_2) are primary air pollutants produced by combustion processes and are harmful to human health. Surface NO_x emissions are emitted from anthropogenic sources, such as fossil fuel combustion in power plants and vehicles, and are primarily in the form of NO [1]. NO_x plays a key role in the photochemical formation of tropospheric ozone (O_3) via photochemical reactions involving volatile organic compounds

(VOCs) and hydroxyl radical (OH) [2,3]. In the case of an alkane (RH), the photochemical reactions proceed as shown in Equations (1)–(4). RH reacts with OH and an oxygen molecule (O_2) to form a peroxy radical, which oxidizes NO. NO_2 photolysis offers NO and triplet oxygen ($O(^3P)$), and $O(^3P)$ reacts with NO_2 to form O_3 with the third body (M).

$$RH + OH + O_2 \rightarrow RO_2 + H_2O \quad (1)$$

$$RO_2 + NO \rightarrow RO + NO_2 \quad (2)$$

$$NO_2 + h\nu\ (\lambda < 420\ \text{nm}) \rightarrow NO + O(^3P) \quad (3)$$

$$O(^3P) + O_2 + M \rightarrow O_3 + M \quad (4)$$

In urban areas, more than 50% of NO_x is concentrated within the planetary boundary layer because surface emission sources dominate for NO_x. NO_x has a short lifetime of several hours and is therefore spatially inhomogeneous. In NO_x-saturated conditions, ozone formation and destruction become sensitive to volatile organic compounds (VOCs), a situation referred to as VOC-limited, whereas in NO_x-limited conditions, they are sensitive to NO_x. Determining the local ozone formation regime is essential for designing effective air pollution mitigation policies. In most urban areas of Japan, the regime is expected to be VOC-limited [4,5]. Recently, Itahashi et al. [6] analyzed 15 years of long-term satellite observation data and reported changes in ozone formation regimes across East Asia, including Japan, particularly after 2015. Based on the observed increase in the ratio of formaldehyde (HCHO) to NO_2 column amounts (HCHO-to-NO_2 ratio; FNR) obtained from satellite measurements, the authors concluded that the regime has gradually shifted from VOC-limited to NO_x-limited. In Tokyo, during the winter season, which is the focus of this study, the number of days classified as NO_x-limited or in a transitional regime was less than 10% between 2005 and 2015. However, it increased to approximately 10–30% from 2015 to 2019. Furthermore, according to Jin et al. [7], although their analysis was performed in the United States, FNR values derived from geostationary orbit satellite observations indicate that ozone formation regimes in major metropolitan areas exhibit diurnal variability: VOC-limited conditions are dominant in the morning when NO_2 concentrations increase, whereas NO_x-limited conditions dominate in the afternoon. Although the photochemical reactions described above lead to O_3 formation during daytime in the vicinity of local emission sources, O_3 is reduced mainly at night by reaction with NO (referred to as NO titration) as shown below:

$$O_3 + NO \rightarrow NO_2 + O_2. \quad (5)$$

Previous studies [8,9] have reported this phenomenon in cities worldwide, including cities in Japan.

Ambient air pollutant concentrations are monitored using a variety of ground-based, airborne, and satellite-based platforms through both in situ measurements and remote-sensing techniques. In Japan, long-term in situ observations of surface concentrations of air pollutants, including NO_x, O_3, sulfur dioxide (SO_2) and non-methane hydrocarbons (NMHCs), have been conducted for several decades by the Ministry of the Environment in Japan and local authorities. These observations provide detailed information on emissions from traffic and on diurnal variations in near-surface concentration, although the monitoring network is spatially sparse. On the other hand, satellite-based remote sensing provides spatially dense two-dimensional images of the slant column density (SCD) and vertical column density (VCD) of NO_2, HCHO and O_3 by observing the radiance spectra within the UV/visible range. In the case of the low-Earth orbit (LEO), however, satellite-based observations have limitations such as coarse temporal resolution and fixed overpass times

depending on the satellite orbits and altitudes. Satellite remote sensing from the LEO has been conducted by Global Ozone Monitoring Experiment (GOME; [10]), SCanning Imaging Absorption SpectroMeter for Atmospheric CHartographY (SCIAMACHY; [11]), the Ozone Monitoring Instrument (OMI; [12]), and the TROPOspheric Monitoring Instrument (TROPOMI; [13]), each offering gradual improvements in spatial resolution down to the kilometer scale. These satellite observations finally provide tropospheric VCD for trace gases. Uncertainties in the tropospheric VCD are dominated by uncertainties in the AMF in a polluted region. Because the ground sampling distances differ among platforms, typically by ~100 m for airborne measurements and ~10 km for ground- and satellite-based measurements, different spatial representativeness must be considered when comparing multi-platform and in situ data.

The coronavirus disease in 2019 (COVID-19) had a major impact on atmospheric composition, including air pollutants and greenhouse gases. With the global spread of COVID-19, lockdown measures were implemented in many cities and countries. In Japan, however, strict legal lockdowns were not imposed; instead, social distancing was encouraged on a voluntary basis. A large outbreak on a cruise ship docked at Yokohama Port (Kanagawa prefecture) may have prompted voluntary restrictions on mobility in Kanagawa prefecture and the surrounding prefectures in February 2020. In addition, COVID-19 spread in Hokkaido prefecture earlier than in other prefectures, leading to a locally declared state of emergency (SoE) there at the beginning of March. Subsequently, a SoE from the Japanese government was declared in seven prefectures, including the Tokyo, Kanagawa, Saitama, and Chiba prefectures (hereafter referred to as the Kanto region regarding these four prefectures), from 7 April 2020 to 25 May 2020.

Global effects of the COVID-19 pandemic on atmospheric composition have been widely reported [14–20] using ground-based/satellite observation, as well as chemical transport models (CTMs). Miyazaki et al. [21] estimated the effects of the COVID-19 lockdown on anthropogenic emissions using a data assimilation approach, reporting that global anthropogenic nitrogen oxide (NO_x) emissions decreased by 9–15% in 2020 relative to total global emissions, with maximum reductions of 24.8% in May 2020, especially in the Middle East and West Asia. Shi et al. [22] reported an abrupt NO_2 decline (10 to 50%) and a concurrent O_3 increase (2 to 30%) in 11 cities globally during the COVID-19 pandemic using site-specific hourly concentration data. In Japan, Damiani et al. [23] investigated the spatiotemporal variability in air pollutants, including NO_2, formaldehyde (HCHO), O_3 and aerosols, in Greater Tokyo mainly using ground- and satellite-based remote sensing data. They found an average 10% reduction in tropospheric NO_2 VCDs and enhancement in the FNR, especially in suburban regions, indicating a shift in the ozone formation regime from VOC-limited to NO_x-limited conditions. However, Phan and Fukui [24] concluded that increases in O_3 concentrations during the COVID-19 pandemic did not occur immediately, although they also observed significant reductions in ambient NO_2 concentrations, ranging from 14.5% to 19.1%, compared with levels in the previous decade (2010–2019). While previous studies have investigated declines in air pollutants and evaluated the impact of the COVID-19 lockdown on atmospheric composition, the variation in baseline O_3 concentrations during COVID-19 remains insufficiently discussed. Moreover, no studies have focused on the diurnal variation in air pollutants during the COVID-19 pandemic.

In this study, we quantified the reduction in NO_2 in a metropolitan area of Japan (Kanto area) using both satellite and ground-based data during the SoE period, which was declared in response to the COVID-19 pandemic. Subsequently, we also examined the $NO_x(NO_2)$-O_3 relationship before and during the COVID-19 pandemic to assess the influence of precursors on O_3 formation. Specifically, we investigated variations in the ozone-formation regime and quantified changes in the baseline O_3 concentration during the pandemic, pro-

viding insights relevant to air-quality policy making. In the following, Section 2 describes mobility changes during the COVID-19 pandemic in the Kanto area (Section 2.1), satellite (Section 2.2) and ground-based (Section 2.3) measurement data, and an analytical method for evaluating the influence of the COVID-19 lockdown on the atmosphere (Section 2.4). Section 3 presents results from satellite and ground-based measurement data (Section 3.1), a consideration of year-to-year trends for trace gases (Section 3.2), and analytical results of the relationship among NO_2, O_3 and NMHCs. Section 4 presents the conclusion of this study and future perspectives.

2. Data and Methods

2.1. Mobility Changes During the COVID-19 Pandemic

To quantify changes in human activity, we used the COVID-19 Community Mobility Reports produced by Google ([25]: https://www.google.com/covid19/mobility/; last access: 1 April 2026). The mobility indices are calculated relative to the median of data collected for each weekday from 3 January to 6 February 2020 across six categories: "Retail and recreation", "Grocery and pharmacy", "Transit stations", "Residents", "Parks", and "Workplaces". Figure 1 presents a time series of mobility change rates for the metropolitan area, the Kanto region in Japan. The gray- and red-shaded terms in Figure 1 indicate the periods of the SoE declared in the Kanto region and for Tokyo only, respectively. Mobility change rates in the "Retail and recreation", "Transit station", and "Workplaces" categories dropped significantly during the SoE periods; conversely, the "Residents" category increased as people worked from home and refrained from going out. Table 1 summarizes the minimum mobility values (maximum for "Residents") in the Kanto region and the demographic data. The Kanto region is a well-urbanized and densely populated region in Japan. Though the ratio of the land area of these four prefectures is 3.59%, about 30% of the population is concentrated in this region. For the mobility change rate, Table 1 shows that human activities, including transportation, decreased to about 65% during the SoE declaration (7 April–25 May 2020).

Table 1. Summary of minimum (or maximum for "Residents") values of mobility change rates (%) during the state of emergency (7 April–25 May 2020) and demographic data of each prefecture.

	Tokyo	**Kanagawa**	**Chiba**	**Saitama**
Sector				
Retail and recreation	−58.6	−40.0	−36.6	−32.0
Grocery and pharmacy	−11.0	−3.0	−4.8	−2.4
Transit stations	−66.8	−60.4	−61.4	−60.6
Residents (maximum)	31.2	28.6	26.0	26.6
Parks	−33.2	−12.2	−18.0	−19.8
Workplaces	−65.2	−61.0	−55.8	−56.6
Demographics				
Population [million]	14.18	9.23	6.25	7.33
(percentage)	(11.45%)	(7.45%)	(5.05%)	(5.92%)
Land area [km^2]	2199.94	2416.55	5156.48	3797.75
(percentage)	(0.58%)	(0.64%)	(1.36%)	(1.00%)

2.2. Satellite Data

2.2.1. OMI

OMI was launched in 2004 on board the Aura satellite. The Aura satellite has a sun-synchronous orbit with a local equator-crossing time of approximately 13:30 local solar time (LST) and observes backscattered solar radiation within the UV–visible spectral range (270–500 nm). OMI retrieves tropospheric NO_2 VCDs with a spatial resolu-

tion of 13 km × 24 km at nadir. In this study, we used the Level-3 daily global gridded product (OMNO2d), which provides tropospheric and total NO_2 VCDs averaged into 0.25° × 0.25° grids. Only pixels with a cloud fraction less than 30% were included in the analysis. The OMNO2d data were downloaded from the NASA Goddard Earth Sciences Data and Information Services Center (GES DISC) (https://disc.gsfc.nasa.gov/; last access: 20 April 2026).

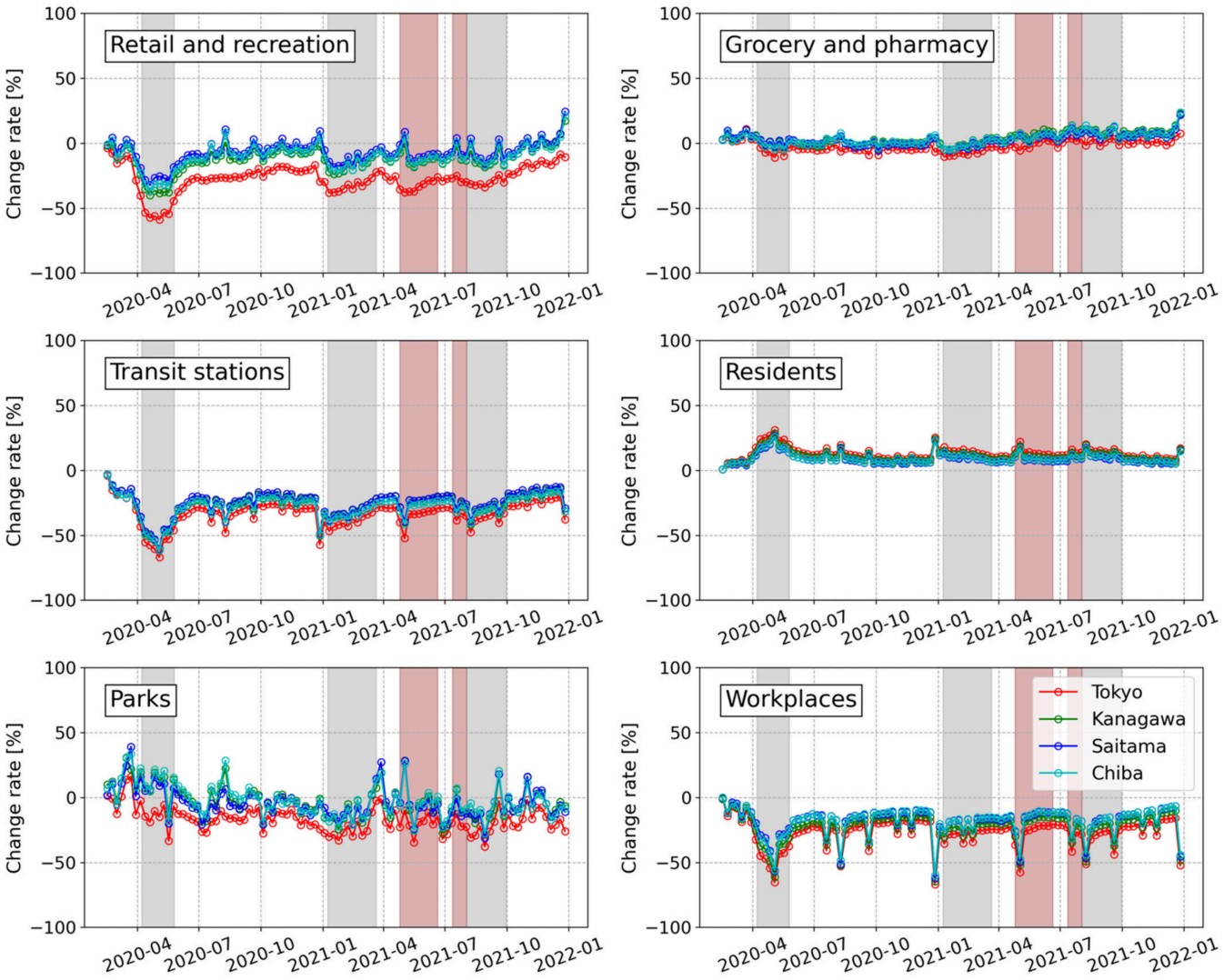

Figure 1. Time series of mobility change rates for each category in four Japanese prefectures (Tokyo, Kanagawa, Saitama, and Chiba). Change rates are calculated based on the median of weekday mobility data for 3 January to 6 February 2020. Gray- and red-shaded areas indicate the periods of the state of emergency declared in all four prefectures and in Tokyo alone, respectively.

2.2.2. TROPOMI

TROPOMI was launched in 2017 on the Sentinel-5 Precursor satellite. TROPOMI employs a measurement concept similar to OMI but with a finer spatial resolution. It provides Level-2 NO_2 VCD data at approximately 7 (5.5) km × 3.5 km. In this study, we used the TROPOMI_MINDS_NO2 product, processed under NASA's Making Earth System Data Records for Use in Research Environments (MEaSUREs) program. This product applies adapted OMI operational algorithms to TROPOMI data, facilitating direct comparison with OMNO2d data. The data are also offered from the NASA GES DISC upon a user registration.

2.3. Ground-Based Data (AEROS)

The Atmospheric Environmental Regional Observation System (AEROS) monitors air pollutants, including NO_x (NO + NO_2), O_3, NMHCs, carbon monoxide (CO), SO_2, suspended particulate matter (SPM), and others. The Atmospheric Environmental Regional Observation System (AEROS) monitoring sites are widely distributed throughout Japan and have measured air pollutant concentrations at hourly intervals since 1970. Figure 2 shows the study area and the locations of AEROS and meteorological observatories used here. To distinguish urban and suburban areas, we defined two analysis areas, indicated by the blue and red dotted rectangles in Figure 2: a blue rectangle (±0.5° in latitude/longitude) centered on Tokyo Station (35.68° N, 139.77° E) representing the suburban area, and a red rectangle (±0.2°) representing the urban area. Not all AEROS sites measure all species. This study used 324 sites for NO_x (NO_2), 210 sites for O_3, and 126 sites for NMHCs. Sites with incomplete data during the target period (January–April 2015–2021) were excluded from statistical analyses. We focused on surface NO_2 (NO_x) and O_3 concentrations to evaluate the impact of the COVID-19 pandemic on atmospheric composition in the Kanto region. Surface NO_2 concentrations in AEROS are measured either by the Saltzman method or a chemiluminescence method (i.e., reaction of NO + O_3). The latter may be affected by contamination from NO_z species (e.g., peroxyacetyl nitrate) because of the use of a nonselective molybdenum converter for NO. Differences in measured NO_2 concentrations between the two methods are shown in Figure S1 in the Supplementary Information. Although mean NO_2 values occasionally show inconsistencies due to NO_z overestimation, median NO_2 values are comparable across months. Some prefectures in the Kanto region use only the Saltzman method to quantify surface NO_2 concentration. Therefore, to maximize data coverage for statistical analyses, we used the median AEROS values in this study. Surface O_3 concentrations were measured by UV absorption. The high-quality data of the O_3 concentrations is assured.

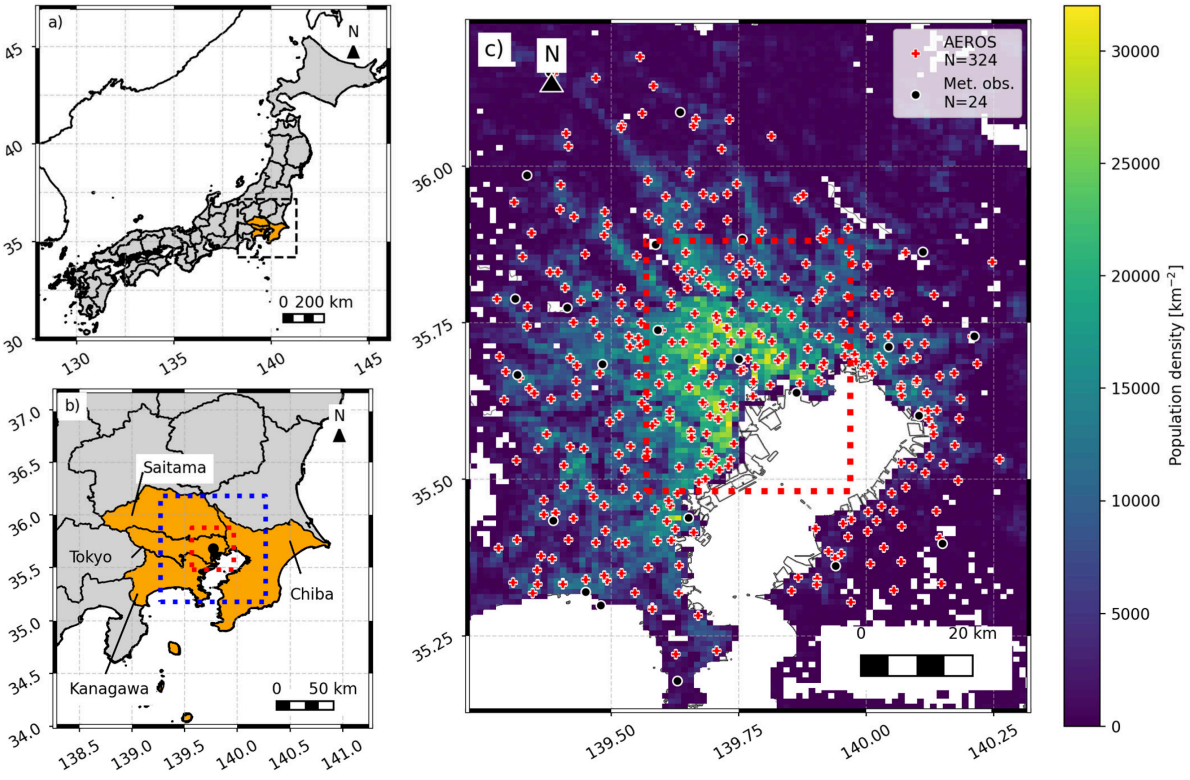

Figure 2. Map of the study area in the Kanto region of Japan. (**a**) The location of the Kanto region (including Tokyo, Kanagawa, Saitama and Chiba prefectures; orange-shaded area). (**b**) Enlarged view

of the Kanto region outlined by the dashed black box in the upper left panel. (**c**) Detailed map of the blue rectangle in the lower-left panel showing AEROS monitoring stations (red plus, N = 324) and meteorological observatories (black circle, N = 24) used in this study. The background color map shows a distribution of population density.

2.4. Analysis of the Influence of the COVID-19 Pandemic on Air Quality

We first analyzed the monthly means of OMNO2d data from 2015 to 2020 to quantify changes in NO_2 column amounts. Data from January to April were extracted to include the period before and during part of the first SoE that was declared in Japan. Only weekday data were used to remove the "weekend effect" attributable to reduced human activity (e.g., industrial operations and transportation) on weekends. Unless otherwise noted, the analyses in this study were conducted excluding weekends as well as public holidays. TROPOMI_MINDS_NO2 data were gridded to 0.05° and compared with OMNO2d data over the blue rectangle area shown in Figure 2. To evaluate differences between TROPOMI and OMI data, we compared monthly mean NO_2 VCDs retrieved by both instruments from January to April during 2015–2019 and in 2020.

To quantify the effect of the COVID-19 pandemic on surface atmospheric composition, we compared AEROS surface NO_2 and O_3 data from January to April before and during the COVID-19 pandemic. For each site, the 2015–2019 monthly medians were treated as a climatology for comparison. Furthermore, we estimated yearly trends in AEROS median NO_2 data using a linear regression model to derive de-trended surface NO_2 concentrations for 2020 and 2021. The linear regression model was used to infer "business-as-usual" (BAU) values during the COVID-19 pandemic, accounting for temporal emission trends and year-to-year variability. A de-trending correction (Section 3.3) was then applied to facilitate comparison between pre- and peri-COVID-19 conditions. To examine baseline changes in O_3 concentrations in the Kanto region during the COVID-19 pandemic, we calculated hourly differences in surface NO_2 (ΔNO_2) and O_3 (ΔO_3) between pre- and peri-COVID-19 periods and compared results for urban and suburban areas separately. Finally, to assess variations in the O_3 formation regime during the COVID-19 pandemic, we analyzed the NMHC/NO_x concentration ratio and calculated potential ozone (PO), which accounts for the effect of NO titration on ozone concentrations.

3. Results and Discussion

3.1. Quantification of the Effect of the COVID-19 Pandemic

3.1.1. Results from Satellite Data

We compared OMNO2d data from January to April 2015–2019 with those from the same months in 2020 during the COVID-19 pandemic. Satellite data within the area highlighted in the panel at the right in Figure 2 were extracted and re-gridded for analysis. Figure 3 shows contour maps of monthly mean OMNO2d averaged over 2015–2019 and 2020, as well as the absolute differences between the two periods. Although OMI has been in operation since 2004, we used the most recent five years (2015 to 2019) as the climatological baseline. This choice avoids large uncertainties in long-term NO_2 trends introduced by major energy demand and policy shifts, such as Japan's response to the Paris agreement adopted in December 2015 and the Great East Japan Earthquake on 11 March 2011. The former, which took effect in 2016, prompted global greenhouse gas reduction targets, while the latter caused drastic changes in Japan's energy policy. Thus, including pre- and post-earthquake NO_2 data in the climatology could obscure recent trends. In most southern coastal areas of Japan, including the Kanto region, tropospheric NO_2 VCDs decreased by more than 1.0×10^{15} molec. cm^{-2} (approximately 10%) from January to March, reflecting annual NO_2 emission reductions near sources. In March, the Kanto region

exhibited a significant decrease, with average reductions of 5.1 × 10^{15} molec. cm^{-2} (38%). These changes were accompanied by an approximately 20% reduction in mobility, as shown in Figure 2.

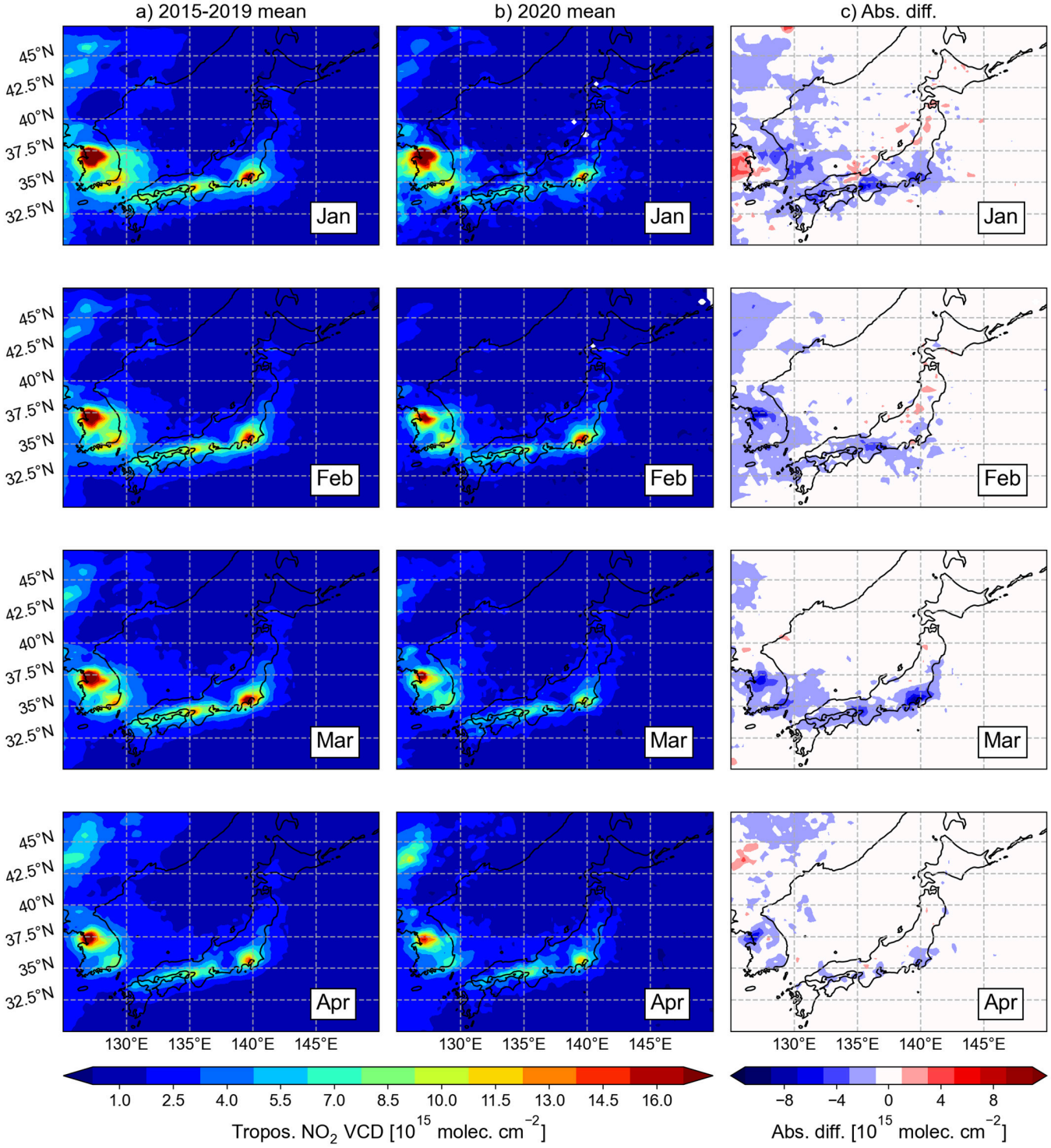

Figure 3. Monthly mean tropospheric NO_2 vertical column densities (VCDs) observed on weekdays by OMI from January to April: (**a**) 2015–2019 climatological means, (**b**) 2020 means, and (**c**) absolute differences (2020 minus 2015–2019). Color bars indicate NO_2 VCDs (**a**,**b**) and absolute differences (**c**) in units of 10^{15} molecules cm^{-2}.

To verify NO_2 reductions with the other satellite measurements and to better understand regional NO_2 reduction patterns at a finer scale, we also generated monthly

gridded maps of TROPOMI NO_2 data at 0.05° resolution for the Kanto region, as shown in Figure 4. Since TROPOMI_MINDS_NO2 data have only been available since 1 May 2018, we compared 2019 and 2020. In March 2020, tropospheric NO_2 VCDs decreased by 3.3×10^{15} molec. cm^{-2} (27%), which is consistent with the OMI results. Interestingly, slight NO_2 enhancements in March appeared in some relatively remote areas. This increase may reflect greater "Parks" mobility in surrounding prefectures as people traveled outside Kanto to maintain social distancing. In January and February, before the SoE, some tropospheric NO_2 VCD pixels were enhanced by 21×10^{15} and 16×10^{15} molec. cm^{-2}, respectively, particularly over central Tokyo. In contrast, March and April exhibited widespread reductions across the region, including central Tokyo. Figure 5 compares tropospheric NO_2 VCDs (TVCDs) from TROPOMI_MINDS_NO2 between 2019 and 2020 using box-and-whisker plots separated into "urban" and "suburban" categories. The urban area is defined as the 0.4° × 0.4° red rectangle centered on Tokyo Station in Figure 2; the suburban area corresponds to the 1.0° × 1.0° blue rectangle excluding the red rectangle. Throughout the study period, NO_2 TVCDs in the urban area were consistently higher (6.4×10^{15} molec. cm^{-2} on average) than in the suburban area, reflecting dense local emission sources (e.g., vehicles). Both urban and suburban mean NO_2 TVCDs increased in January and February but decreased significantly in March 2020. As shown in Figure 5a, mean values in March decreased by an average of 6.0×10^{15} molec. cm^{-2} (32%) in the urban area and 2.6×10^{15} molec. cm^{-2} (24%) in the suburban area; in April, decreases were 4.1×10^{15} molec. cm^{-2} (24%) and 1.8×10^{15} molec. cm^{-2} (22%), respectively (Figure 5b). These results indicate that NO_2 reductions in an urban area were closely associated with decreased human mobility. Damiani et al. [23], using TROPOMI standard products, reported 20–40% NO_2 reductions during the SoE in southern Tokyo. Although the study periods differ slightly, our results are consistent with those results.

Next, we compared the NO_2 TVCDs observed by OMI and TROPOMI during the same period, as shown in Figure 5. To increase the sample size and simplify the comparison, data from urban and suburban areas were aggregated. Figure 6 presents the mean values of OMI and TROPOMI NO_2 VCDs averaged over the Kanto region (blue rectangle in Figure 2) from January to April before and during the COVID-19 pandemic. For TROPOMI, mean values in January and February between 2019 and 2020 were almost comparable or, in February 2019, lower than 2020 because NO_2 TVCD in 2019 was especially lower than in the previous four years from 2015 to 2018, even considering the NO_2 decreasing trend. Significant NO_2 TVCD declines were also confirmed by the yearly trend of OMI in the upper panels of Figure 10. For OMI, however, mean values in January and February showed a large decline in 2020 compared with those in 2015–2019, which is reasonable based on the NO_2 decreasing trend. In March and April of 2020, during the COVID-19 pandemic, large reductions were evident for TROPOMI, with decreases of 3.3×10^{15} molec. cm^{-2} (27%) and 2.3×10^{15} molec. cm^{-2} (22%), respectively. For OMI, a significant reduction of 5.1×10^{15} molec. cm^{-2} (38%) can be seen in March, whereas the reduction in April was 1.7×10^{15} molec. cm^{-2} (16%), which was comparable with those in January and February, possibly due to shorter NO_2 lifetime in April, an effect arising from five-year averaging and the relatively coarser spatial resolution of OMI (spatial smoothing effect; [26]).

These comparisons of NO_2 column data clearly indicate that the significant reductions observed over the Kanto region were caused by COVID-19-related decreases in human activities, although interannual meteorological effects were not explicitly considered in these analyses. By aggregating the data monthly over a wide 1° × 1° grid, potential influences from meteorological variability and episodic high-NO_2 inflows (e.g., long-range transport) are considered to be minimized.

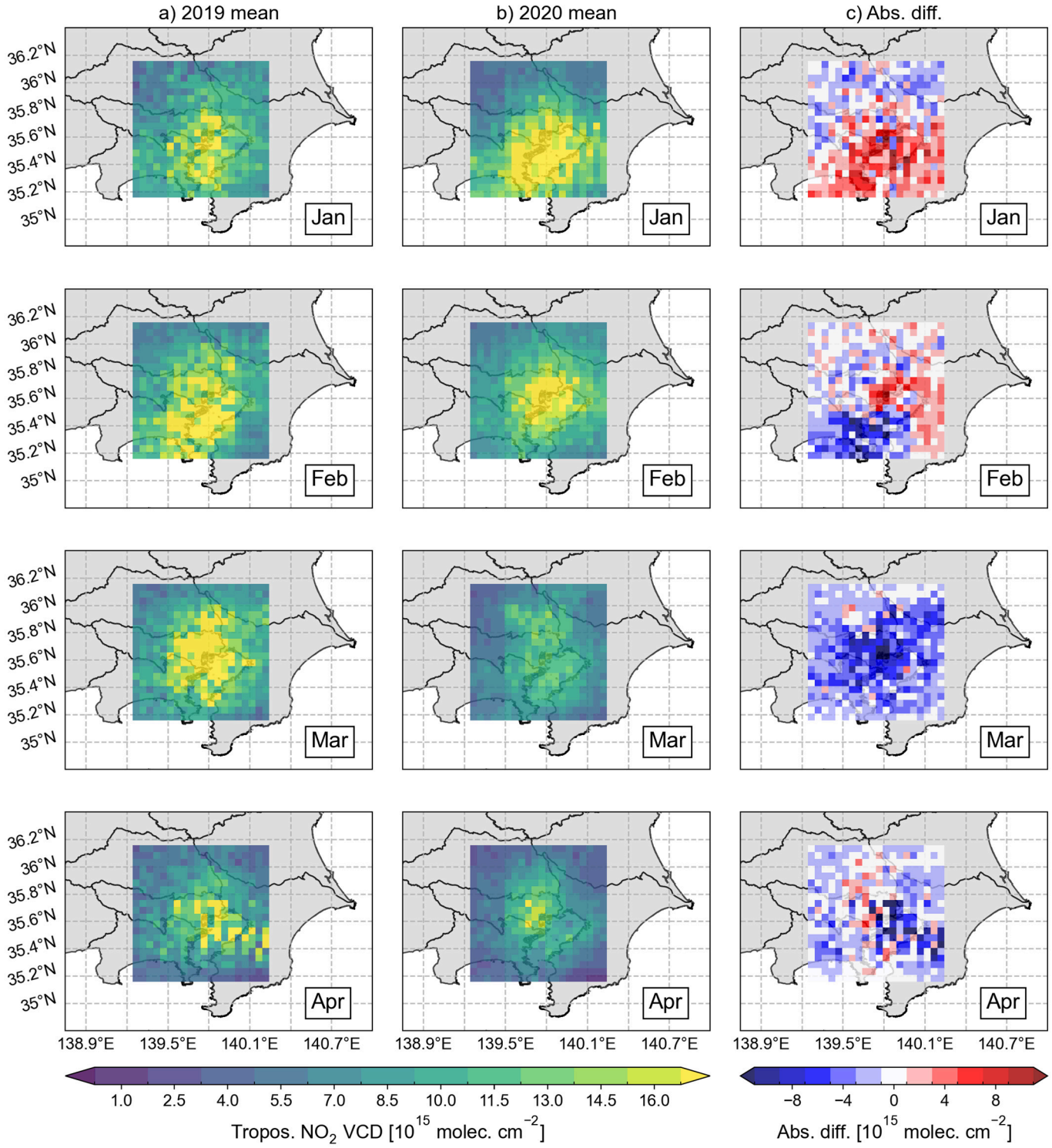

Figure 4. Monthly mean tropospheric NO_2 vertical column densities (VCDs) observed by TROPOMI on a 0.05° × 0.05° grid over the Kanto region (blue rectangle area in Figure 2) centered on Tokyo station (1° × 1°): (**a**) 2019 means, (**b**) 2020 means, and (**c**) absolute differences (2020 minus 2019). Color bars indicate NO_2 VCDs (**a**,**b**) and absolute differences (**c**) in units of 10^{15} molecules cm^{-2}.

3.1.2. Results from Surface Data

To assess COVID-19-related effects on surface concentrations of NO_2 and O_3, we analyzed AEROS data from the Kanto region. To make the comparison with satellite data easier, 2015–2019 data were treated as climatology and compared with data from 2020 and 2021. Figure 7 shows maps of the monthly daytime median NO_2 surface concentrations in

units of parts per billion by volume (ppbv) monitored by AEROS from January to April for 2015–2019 and 2020, together with the absolute differences between the two periods. As with the satellite results, higher NO_2 concentrations were observed closer to central Tokyo. In January, some sites showed increases in surface NO_2 concentration, even within central Tokyo, despite the overall downward trend in NO_2 over recent years. From February to April, widespread decreases in NO_2 surface concentration were evident across the Kanto region, including relatively remote areas except parts of Chiba prefecture. Reductions ranged from 2 to 3 ppbv (12–22%) with maximum decreases of 14 ppbv (100%) in some locations. Cooper et al. [27] investigated regional NO_2 changes during lockdowns across the globe using TROPOMI-derived ground-level NO_2 concentrations. They found that the monthly population-weighted mean difference was −1.9 ppbv between 2019 and 2020 in Japan. The NO_2 declines observed in the AEROS data in this study are consistent with the reductions reported by them.

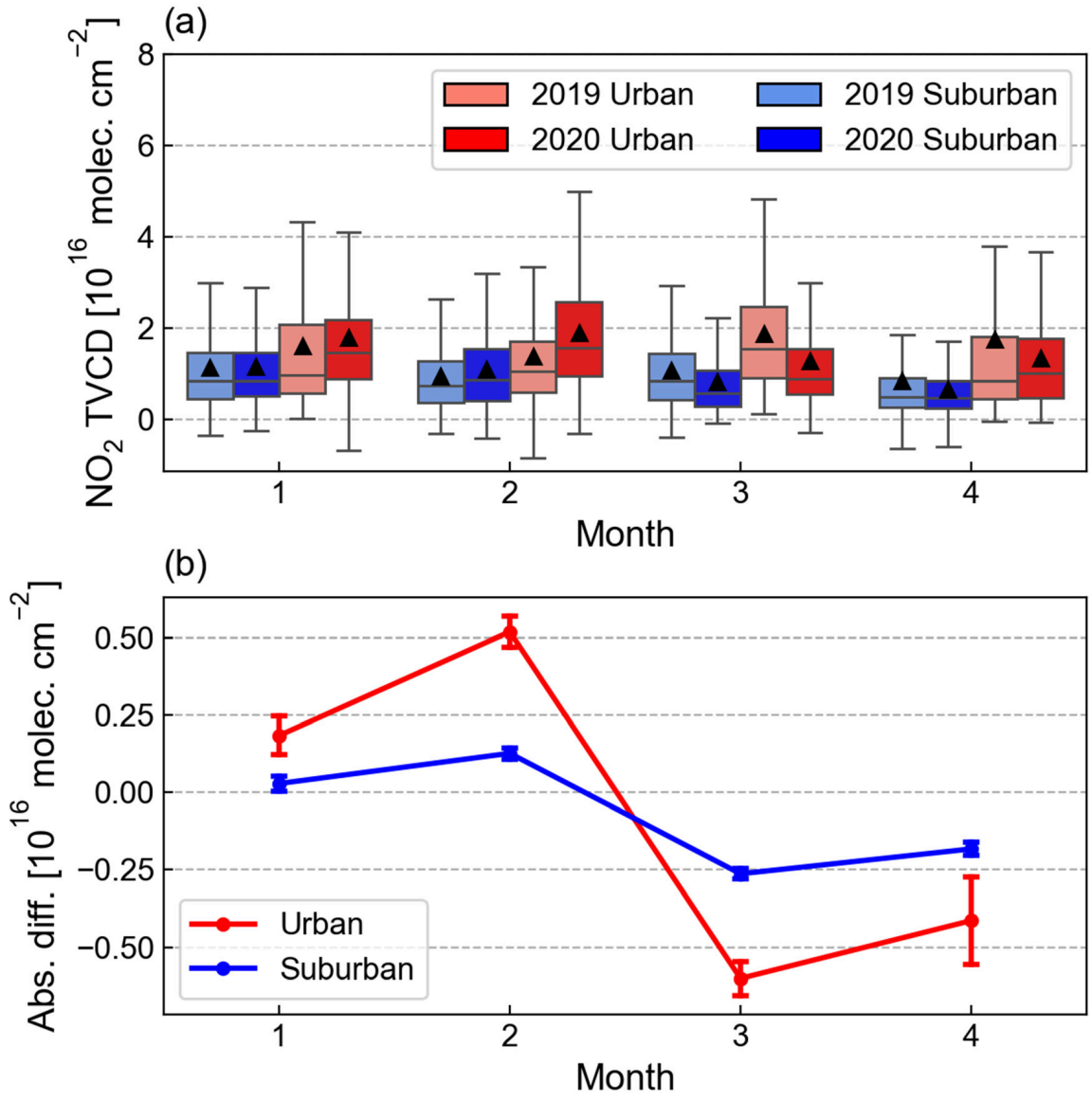

Figure 5. (**a**) Boxplots of tropospheric NO_2 vertical column densities (VCDs) observed by TROPOMI from January to April. Warm-colored boxes show "urban" sites and cool-colored boxes show "suburban" sites (see text for definitions). Light colors indicate 2019, and darker colors indicate 2020. Solid triangles represent the means, and horizontal lines represent the medians. (**b**) Absolute differences and standard deviations between 2019 and 2020 (2020 minus 2019) for urban and suburban sites.

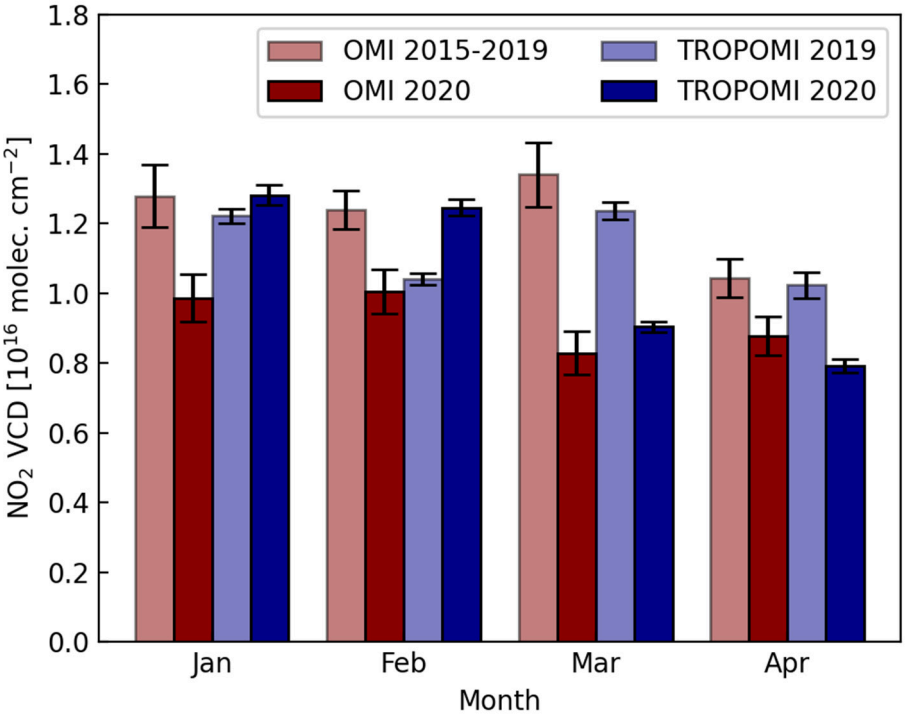

Figure 6. Comparison of monthly mean tropospheric NO_2 vertical column densities (VCDs) from OMI and TROPOMI averaged over the 1° × 1° area (blue rectangle in Figure 2). Warm-colored bars show OMI data for 2015–2019 (light) and 2020 (dark), while cool-colored bars show TROPOMI data for 2019 (light) and 2020 (dark). Error bars indicate the monthly standard errors for each measurement.

Figure 8 shows the same type of plots as Figure 7, but for O_3. Surface O_3 concentration exhibits more complex variations compared to NO_2. In January and February, a decreasing trend in surface O_3 was observed along the coastal areas of Kanagawa and Chiba prefectures. Furthermore, while an overall decline was evident in March, the O_3 concentration in April showed an increasing trend at most sites, with a few exceptions. However, these tendencies varied considerably among sites; some locations in Kanagawa and Chiba, as mentioned above, continued to exhibit a decreasing trend. Figures 7 and 8 indicate that, except for March, the O_3 formation regime is, in general, VOC-limited at most sites since O_3 concentrations tend to increase as NO_2 decreases (and vice versa). Considering this relationship between NO_2 and O_3, the declining trend of O_3 observed in March is particularly noteworthy.

As shown in Figures 7 and 8, because the observation sites where high NO_2 (low O_3) concentration was observed are spatially inhomogeneous, though NO_2 basically tends to be high closer to central Tokyo, an additional condition was applied to extract substantial urban sites; sites exceeding 60-percentile NO_2 of all targeted periods and sites were assigned as urban. After applying this threshold, though the number of sites assigned as urban became 13% of the total, it was enough to perform a statistical analysis. Hereafter, unless otherwise noted, we apply this threshold. Figure 9 shows boxplots of the monthly daytime AEROS surface NO_2 and O_3 concentrations separated into urban and suburban regions for 2015–2019, 2020, and 2021. Both surface NO_2 and O_3 medians in March 2020 decreased relative to 2015–2019, by 4.5 ppbv and 1.5 ppbv in the urban area and 2.0 ppbv and 1.5 ppbv in the suburban area, respectively. Furthermore, in the urban area, the upper whisker of the boxplots (i.e., maximum value less than 1.5 times the interquartile range above the 75th percentile) decreased markedly in 2020 by 17.0 and 12.5 ppbv for NO_2 in March and April, respectively. These declines are likely attributable to reduced human activity, since the range between the lower and upper whiskers and median values was significantly decreased in

March and April of 2020 and 2021. This behavior can also be seen in the suburban area. For surface O_3, the variability in surface concentration (i.e., the difference between the lower and upper whiskers) in March and April 2020 was lower than during 2015–2019, while the mean and median O_3 values were comparable between the two periods. This may indicate that surface O_3 approached a photostationary state with NO_x under reduced VOC levels, that meteorological variability (winds and humidity/water vapor) was lower during the COVID-19 pandemic, or a combination of both. In the suburban area, NO_2 and O_3 exhibited similar patterns to those in the urban area, though the magnitudes of the changes differed. Interestingly, while O_3 concentrations in 2020 were comparable to, or lower than, climatological values, those in 2021 increased in both the urban and suburban areas in February and March. During the same period, since NO_2 showed significantly lower values, this may be attributable to the weakening of the NO titration. Detailed statistics for urban and suburban sites are summarized in Tables S1 and S2, respectively, in the Supplementary Information.

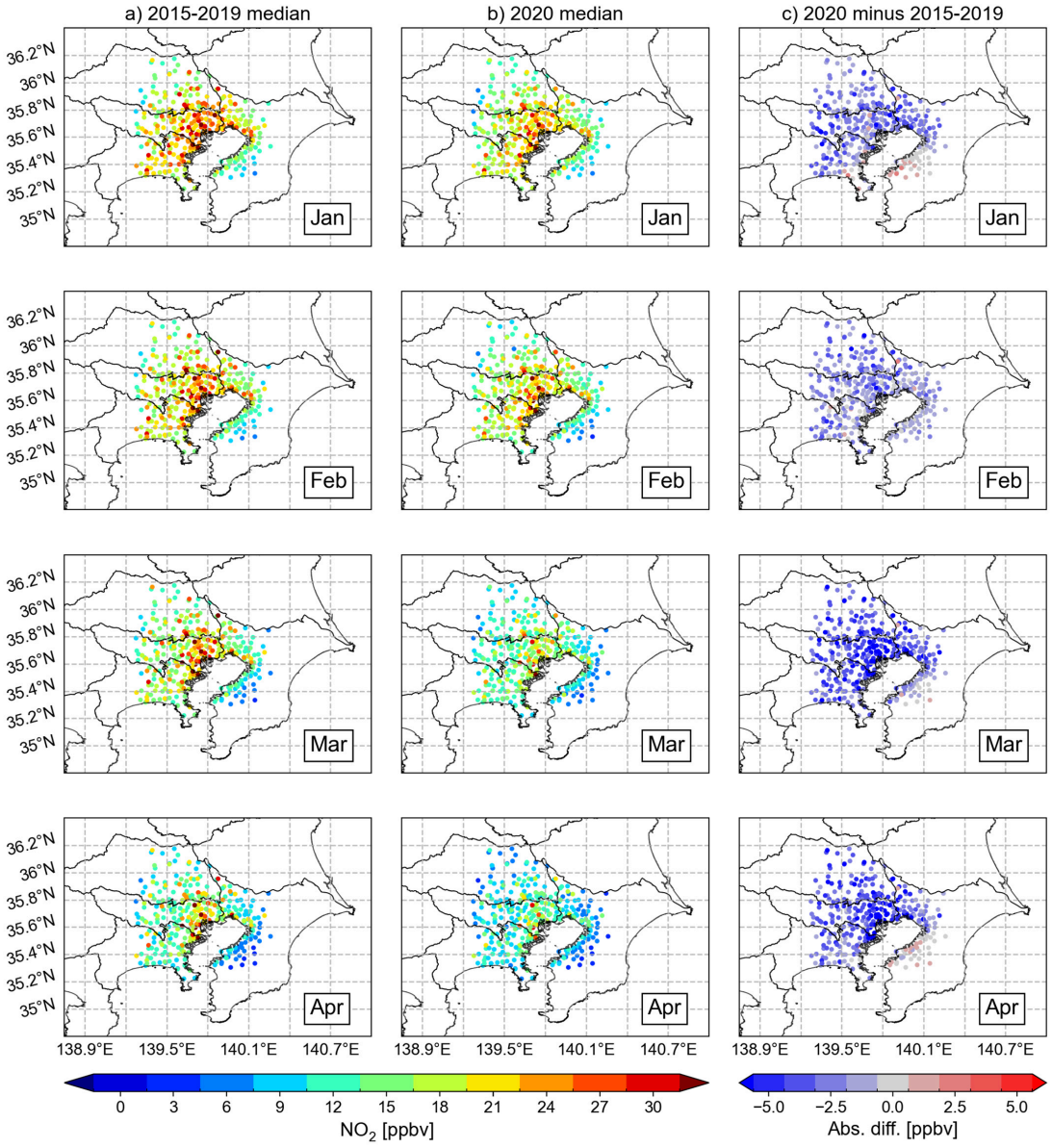

Figure 7. Spatial distribution of the monthly median of NO_2 surface concentrations (ppbv) monitored by AEROS from January to April: (**a**) 2015–2019 climatological medians, (**b**) 2020 medians, and (**c**) absolute differences (2020 minus 2015–2019).

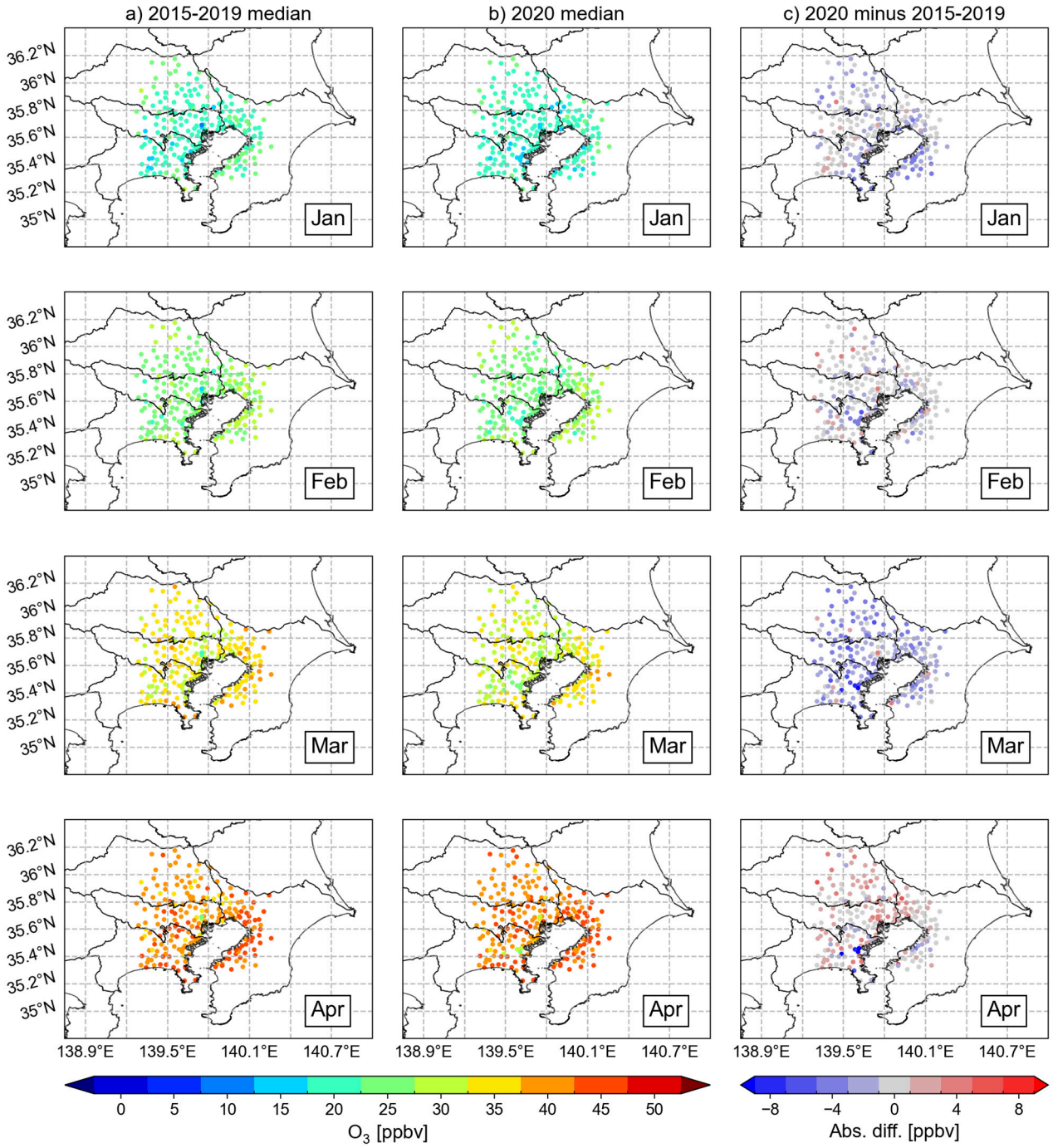

Figure 8. Spatial distribution of the monthly median of O_3 surface concentrations (ppbv) monitored by AEROS from January to April: (**a**) 2015–2019 climatological medians, (**b**) 2020 medians, and (**c**) absolute differences (2020 minus 2015–2019).

3.1.3. Comparison Between Satellite and Ground-Based Data

To compare NO_2 reductions during the COVID-19 pandemic derived from satellite and ground-based measurements considering long-term temporal trends, we applied a simple linear model to estimate the expected NO_2 levels for each month based on year-to-year trends using the OMI and AEROS data. Figure 10 shows a result of the year-to-year trend analysis for OMI NO_2 TVCDs and AEROS surface NO_2 concentrations for January to April from 2015 to 2021. Yearly median values were normalized to those of 2015 and are plotted as open rectangles connected by thick lines. The broken lines and dotted lines show the linear regression results between 2015 and 2019 and extrapolated values in 2020 and

2021, respectively. The extrapolated values in 2020 and 2021 are indicated by solid circles, and the error bars show mean absolute errors (MAEs) of the linear regressions. Different colors correspond to results obtained for the AEROS urban and suburban areas and the OMI results. For the AEROS data, we extracted sites corresponding to the observation sites located within the blue rectangle shown in Figure 2 and averaged observations between 13:00 and 14:00 LST to match OMI's overpass time at 13:30 LST. Japan's decreasing trend in NO_x emissions is well documented [28], and Figure 10 reveals a similar decreasing trend in NO_2 in the Kanto region, except for March. Depending on the period and area, the decreasing trend ranged from −1 to −10% per year. For the OMI data, February 2020 NO_2 values (open rectangles) were close to the extrapolated BAU values and within the MAE range, indicating that NO_2 levels in those months were not yet affected by the COVID-19 pandemic. In March 2020, however, all observed NO_2 values dropped markedly and fell outside the MAE. A similar sudden drop was seen in the AEROS March results, despite an increasing trend in the suburban area. In April, no extreme reductions were observed in the results of this study. By contrast, Phan and Fukui [24] reported NO_2 reductions of 12.9–18.0% between April and May during the first SoE (7 April–25 May) compared with estimated conditions using a machine learning approach. The difference in our findings may arise because we limited the AEROS data to 13:00–14:00 LST and explicitly accounted for the yearly trend.

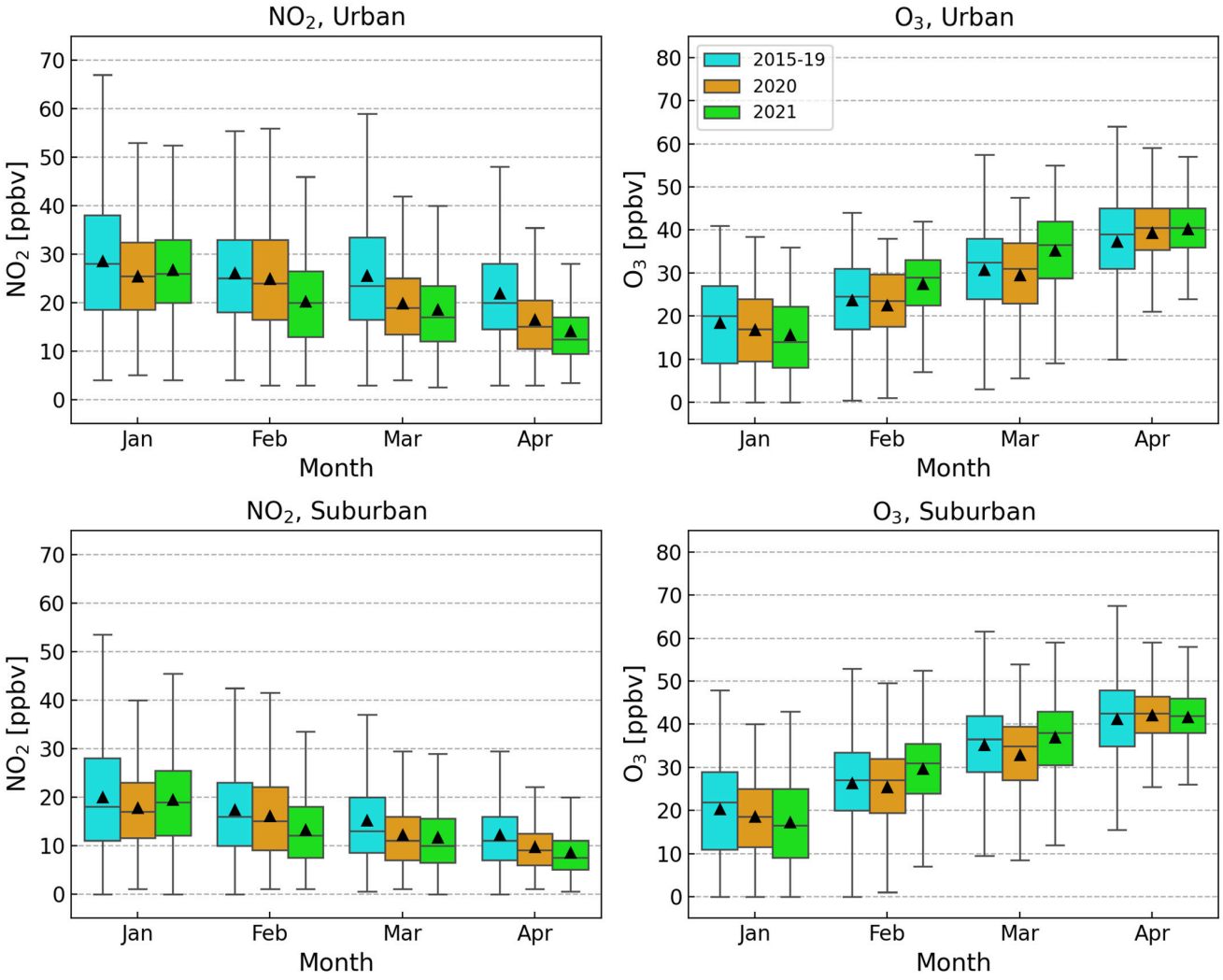

Figure 9. Monthly boxplots of AEROS surface NO_2 and O_3 concentrations in the Kanto region for 2015–2019, 2020, and 2021 in urban sites (**upper row**) and suburban sites (**lower row**).

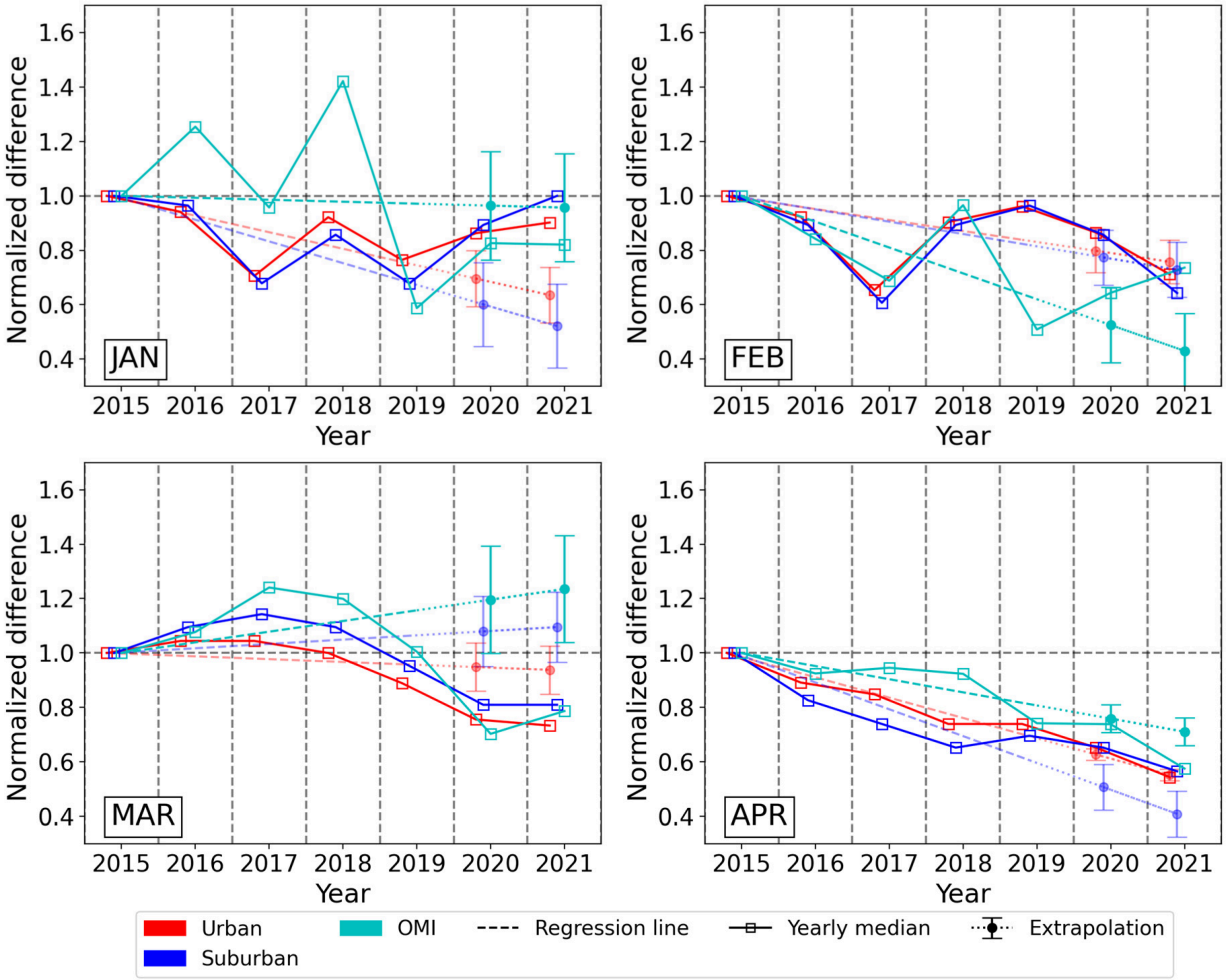

Figure 10. Yearly trends of normalized NO_2 differences (relative to 2015) from January to April for OMI and AEROS.

3.2. Year-to-Year Trend Analysis Considering Meteorological Field

Cooper et al. [27] estimated meteorological effects on NO_2 concentrations for numerous cities worldwide, including those examined in this study (e.g., Tokyo), using GEOS-Chem model simulations at 2° × 2.5° resolution. Estimated NO_2 concentrations were down-scaled to 1 km × 1 km resolution using the horizontal variability in TROPOMI-derived surface concentrations. According to their simulations, meteorology-attributable changes between 2019 and 2020 averaged −9.1 ± 2.4%, accounting for approximately 25–33% of the TROPOMI-observed NO_2 reductions in March and April. If these simulations can be applied to our comparison of 2015–2019 versus 2020 AEROS data, meteorological effects would correspond to approximately 40–75% of the observed reductions across the whole Kanto region, from February to April, indicating that a substantial portion of the surface concentration decrease may be meteorology-driven. The simple linear model used in this study considered only temporal variation in air pollutants and did not explicitly include meteorological variability. To take the meteorological field into account, we also estimated the BAU concentration of air pollutants, including NO_2, NO_x, O_3 and NMHCs, using a Generalized Linear Model (GLM) with meteorological fields as explanatory variables. We then compared the GLM-based BAU estimates with those from the simple linear model. The two models produced consistent results; therefore, for subsequent analyses, we used the simple linear model to estimate de-trend values based on the year-to-year variation. Details of the comparison methodology and results are provided in S2 of the Supplementary Information, as they are outside the focus of this paper. It should be noted that, within the

GLM framework, it is difficult to separately identify the effects of individual meteorological variables on air pollutants during the COVID-19 pandemic because the model assumes non-linear relationships via the link function, and the meteorological variables are not perfectly independent.

Hourly de-trended values ($\gamma_{de-trend}$) were calculated by subtracting an hourly correction factor (δ_{cor}) from the observed concentration (γ_{obs}):

$$\gamma_{de-trend} = \gamma_{obs} - \delta_{cor} \because \delta_{cor} = \gamma_{ext} - \gamma_{2017} \quad (6)$$

where γ_{ext} is the extrapolated (BAU) value, for 2020 or 2021, from the linear regression and γ_{2017} is the interpolated value for 2017. This approach was introduced to remove yearly trends when comparing surface concentrations observed before and after the COVID-19 pandemic. The results of the yearly trend analysis for NO_2 and O_3 are provided in Figure S2 in the Supplementary Information. The correction factors for NO_2, O_3, and NMHCs are shown in Figure S5 in the Supplementary Information.

3.3. Analysis of the Interaction Between NO_2, O_3 and NMHCs During the COVID-19 Pandemic

Figure 11 shows the diurnal variations in AEROS NO_2, O_3, and NMHCs observed on weekdays in March for the urban area. Since the most pronounced NO_2 decrease occurred in March, we focus hereafter on March AEROS surface concentrations. In the upper panels of Figure 11, the broken lines represent hourly data for each year from 2015 to 2019, while the solid lines represent hourly data for 2020 and 2021 without correction for year-to-year variation. In the lower panels of Figure 11, the black dots and dashed lines indicate mean values with standard deviations for 2015–2019 (grey shaded area), and the solid circles and lines show de-trended hourly data for 2020 and 2021 after correcting for interannual trends using a linear regression model.

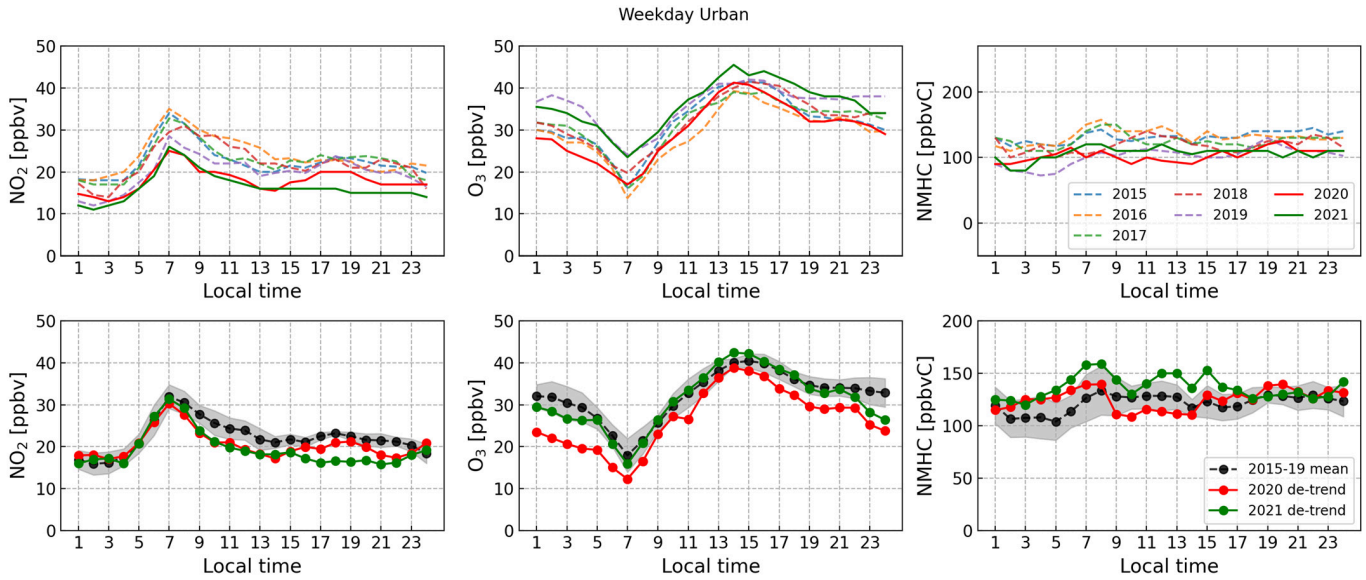

Figure 11. Diurnal variations in NO_2, O_3, and NMHCs observed by AEROS in March on weekdays at sites in the "urban" areas of the Kanto region. Monthly medians of NO_2, O_3, and NMHCs for each year without de-trending are in the top row; 2015–2019 means with mean absolute errors and de-trended NO_2, O_3, and NMHCs observed in 2020 and 2021 are in the bottom row.

For NO_2, the de-trended AEROS surface concentrations during daytime, especially from 9:00 to 15:00, in 2020 were on average 3.9 ppbv (16.3%) lower than in 2015–2019. In 2021, NO_2 from 9:00 to 22:00 local time remained lower by 4.7 ppbv (20.7%) on average. Since the mean standard deviation of the AEROS daytime observations between 2015

and 2019 was 2.0 ppbv, these reductions in the de-trended values can be attributed to COVID-19 lockdown effects, even after accounting for the yearly trend. In contrast, at other times in 2020, the de-trended NO_2 concentrations were almost comparable to those in 2015–2019. Typically, the NO_2 surface concentration in Tokyo exhibits two peaks—one in the morning and another in the evening—with the morning peak being higher than that in the evening [4]. In 2020, NO_2 concentrations exhibited this diurnal pattern more clearly than in 2021. Similarly, NO_x concentrations showed the same diurnal variation as NO_2, as shown in Figure S4. NMHCs showed a more ambiguous diurnal variation compared to NO_2 despite having a slight peak at morning. The decrease during daytime and subsequent increase after evening reflected changes in industrial activities and solar radiation, as anthropogenic sources are assumed to dominate NMHCs in urban areas. It is interesting that de-trended NMHC concentrations in 2021 were relatively higher than the 2015–2019 mean, whereas NO_2 concentrations remained comparable or lower. The elevated NMHC concentrations are likely to be caused by either uncertainties due to the de-trend correction factor or uncertainties due to the lack of considering an advection effect in the de-trend method because, as shown in Figure S5 in the Supplementary Information, variation in the correction factor of NMHCs is large, leading to an overestimation.

In contrast to NO_2, surface O_3 concentrations typically increase after sunrise and reach a peak in the afternoon as solar radiation increases [29]. The observed diurnal patterns of NO_2 and O_3 in this study were both consistent with the results previously reported. In the urban area, whole-day O_3 concentrations in 2020 were on average 5.4 ppbv (18.2%) lower than in 2015–2019, with maximum reductions of 9.8 ppbv (33.4%). During nighttime (01:00–07:00 and 23:00–24:00), hourly O_3 concentrations in 2020 were significantly lower, by an average of 8.4 ppbv (29.7%), compared to those in 2015–2019. In these periods, as NO_2 concentrations were comparable at night but lower during daytime compared to those in 2015–2019, daytime O_3 was more effectively consumed via the reaction described in Equation (5). By 2021, O_3 concentrations had recovered to levels comparable to 2015–2019, possibly because the linear regression model underestimated the climatological year-to-year variation in O_3 for 2021 (see Figure S3).

Figure 12 shows the same type of plots as Figure 11, but for the suburban area, allowing comparison with the urban results. As shown in the upper panels of Figure 12, interannual variability in the suburban area was lower than that in the urban area for all species examined. Although suburban NO_2 surface concentrations in 2020 and 2021 were generally comparable to 2015–2019 levels, daytime (09:00–15:00) NO_2 decreased by 2.3 ppbv (−18.9%) in 2020 and 2.2 ppbv (−18.2%) in 2021. These reductions indicate a clear effect of the COVID-19 pandemic on air pollutants, even in suburban areas where NO_2 levels are typically low. Overall, diurnal patterns and the relationships between pre- and peri-COVID-19 NO_2 concentrations in the suburban area resembled those in the urban area despite the lower absolute NO_2 levels. For O_3, the maximum in the suburban area in 2015–2019 was 47.3 ppbv at 15:00, compared with 40.5 ppbv during the same time in the urban area, a 6.8 ppbv higher peak that is consistent with the results of [28,30]. In 2020 and 2021, however, the absolute differences in maximum O_3 concentrations between the suburban and urban areas (i.e., suburban minus urban) narrowed to 3.9 ppbv and 3.8 ppbv, respectively. This suggests that NO titration by vehicle emissions decreased due to the reduced NO_x emissions in the urban area, leading to more comparable NO_2 concentrations across urban and suburban sites. By 2021, suburban O_3 concentrations recovered to 2015–2019 levels, except at around midnight. In contrast to the urban results, daytime NMHC concentrations in the suburban area in 2020 were lower than in 2015–2019 (except from 07:00 onward), which also likely contributed to reduced O_3 formation.

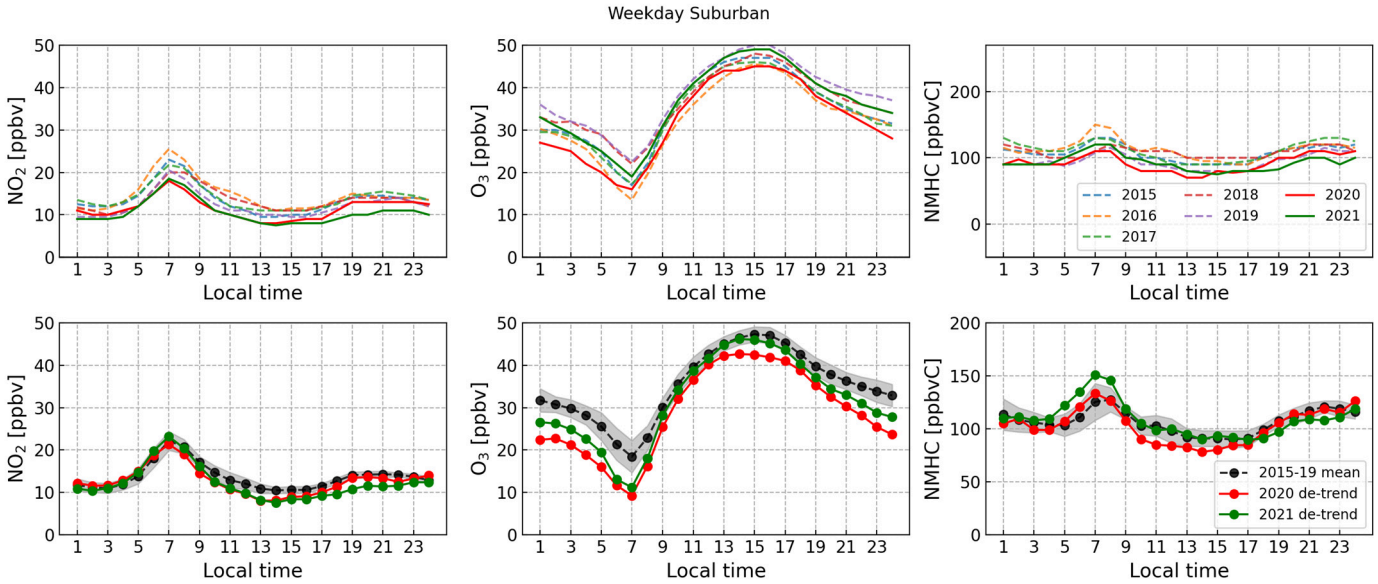

Figure 12. Diurnal variations in NO_2, O_3, and NMHCs observed by AEROS in March on weekdays at sites in "suburban" areas of the Kanto region. Monthly medians of NO_2, O_3, and NMHCs for each year without de-trending are in the top row; 2015–2019 means with mean absolute errors and de-trended NO_2, O_3, and NMHCs observed in 2020 and 2021 are in the bottom row.

Figures S6 and S7 in the Supplementary Information show the year-to-year trend of diurnal minimum, maximum and δO_3 (differences between minimum and maximum) values for each year in the urban and suburban areas, respectively. It should be noted that all the minimum O_3 values were observed at 7:00, and de-trended minimum values in 2020 and 2021 were significantly lower by 5.6 ppbv and 2.0 ppbv in the urban area and by 9.2 ppbv and 7.3 ppbv in the suburban area, respectively, than those in 2015–2019, which was consistent with an increase in the de-trended NO peak at the same time, as shown in Figure S5. In both the urban and suburban areas, δO_3 values slightly decreased from 2015 to 2019, whereas the minimum and maximum values increased starting in 2016, indicating that the yearly baseline O_3 increased since 2016 though the O_3 amount formed and destructed daily was unchanged. Interestingly, however, the de-trended δO_3 values for 2020 (2021) increased by 5.5 (5.0) ppbv in the urban area and 3.8 (6.1) ppbv in the suburban area compared to the 2015–2019 values, which may indicate that local ozone production likely intensified during the COVID-19 pandemic. Itahashi et al. [31] investigated variation in different timescale O_3 values in April and May during the COVID-19 pandemic using CTM and AEROS. They reported that domestic emission reductions increased the monthly daytime mean of O_3 while decreasing the monthly maximum of the daytime peak during the COVID-19 pandemic. Our results were consistent with their results despite differences in targeted periods and analytical methods. According to Gkatzelis et al. [32] and references therein, at most sites around the world, O_3 increased on a regional scale during COVID-19 lockdowns, with a median change of 6.4%, whereas NO_2 decreased. Heald et al. [33] concluded that, in polluted regions, an increase in O_3 concentration arises from two factors: one is catalytic ozone production due to RO_2 radicals under VOC-limited conditions, and another is the weakened NO titration effect. As described in the Introduction, since the Kanto regions including the Greater Tokyo area are often observed as VOC-limited, our results showed a different behavior from those previously reported in urban/polluted areas.

Next, in order to estimate the net change in O_3 levels before and during the COVID-19 pandemic and changes in the O_3 formation regime, we compared NMHC/NO_x and introduced potential ozone (PO), defined as

$$PO = O_3 + NO_2 - \alpha NO_x, \quad (7)$$

where α is the fraction of primary NO_2 contained in NO_x. PO represents the net O_3 concentration, accounting for photochemical production and transport without the influence of NO titration, under the assumption that the sum of O_3 and NO_2 in Equation (5) is conserved [9,34]. Following previous studies [30,35], we used α = 0.1, which is broadly accepted in Japan. Figure 13 shows diurnal variations in NMHC/NO_x and PO values in the urban and suburban areas. According to [4] and references therein, the boundary region between NMHC- (VOC) and NO_x-limited regimes corresponds to an NMHC/NO_x of 8–10 ppbvC/ppbv. It should be noted that a determination of the O_3 formation regime using NMHC/NO_x has a large uncertainty because the boundaries of NMHC- and NO_x-limited regimes and the boundary region vary depending on location and season [36,37]. Liu et al. [36] showed analysis results of the O_3 formation regime with NMHC/NO_x using the classical Empirical Kinetic Modeling Approach in four sites of Taiwan and estimated lower and upper bounds of the boundary region during winter to be 2.22–8.11 and 6.45–12.96, respectively. Interestingly, the range we assumed is slightly consistent with the calculated range of bounds, 5.14 ± 2.19–9.85 ± 2.31 ppbvC/ppbv, although they showed large variation. In the Kanto region, including both the urban and suburban areas, no period of the day fell into the NO_x-limited regime. In the urban area, ozone formation remained VOC-limited throughout the day. In the suburban area, VOC-limited conditions extended from 04:00. In the morning, when surface NO_2 concentrations peak, the regime consistently tended toward VOC limitation.

The right panels in Figure 13 show the diurnal variation in PO values in the urban and suburban areas. In the urban area, an overall PO reduction due to the COVID-19 lockdown was evident in 2020, while in 2021, the reduction was less pronounced and PO values approached those in 2015–2019. In the suburban area, however, PO values in 2021 remained low and comparable to those in 2020, indicating slower recovery of human activities, likely due to ongoing mobility restrictions in suburban regions. On average, the differences in PO between 2020 and 2015–2019 were −6.3 ppbv in the urban area and −7.1 ppbv in the suburban area. In 2021, the corresponding differences were −3.2 ppbv and −4.7 ppbv, respectively. These values indicate that photochemical O_3 decreased by 6.7 ppbv in 2020 and 4.0 ppbv in 2021, compared with 2015–2019 in the Kanto region.

Total uncertainties in PO were affected not only by measurement errors but also an estimation error of α. The fraction of primary NO_2 (i.e., α) changes with vehicle types, the Euro standard class (Euro 1 to Euro 7), which is an emission standard determined by European Union governments and adopted internationally, and the mix of vehicles with different control technologies [38–40]. In Japan, the original emission regulation complies with the Euro standard class. Brimblecombe et al. [41] reported that α increased from 2008 up to about 0.2 in 2014, and it decreased down to below 0.1 recently (around 2020) in Hong Kong. Minoura and Ito [42] reported an α value of 0.073 by using in situ measurement implemented in Tokyo, Japan. However, measurements to determine the α value are basically limited in Japan so far, especially in the last decade. Furthermore, previous studies [40,41] reported that recent high-level regulations, such as Euro 6, lead to higher α values compared with a lower level of Euro classes. Therefore, a lack of measurements for primary NO_2 in Japan and consequent assumption of α = 0.1 possibly leads to large uncertainty in consideration of primary NO_2, which results in the underestimation of primary NO_2 and subsequent overestimation of PO. Thus, the absolute amplitude of the

PO reduction in 2020 and 2021 may need to be evaluated carefully. However, the qualitative conclusion that PO decreased during the COVID-19 pandemic is robust.

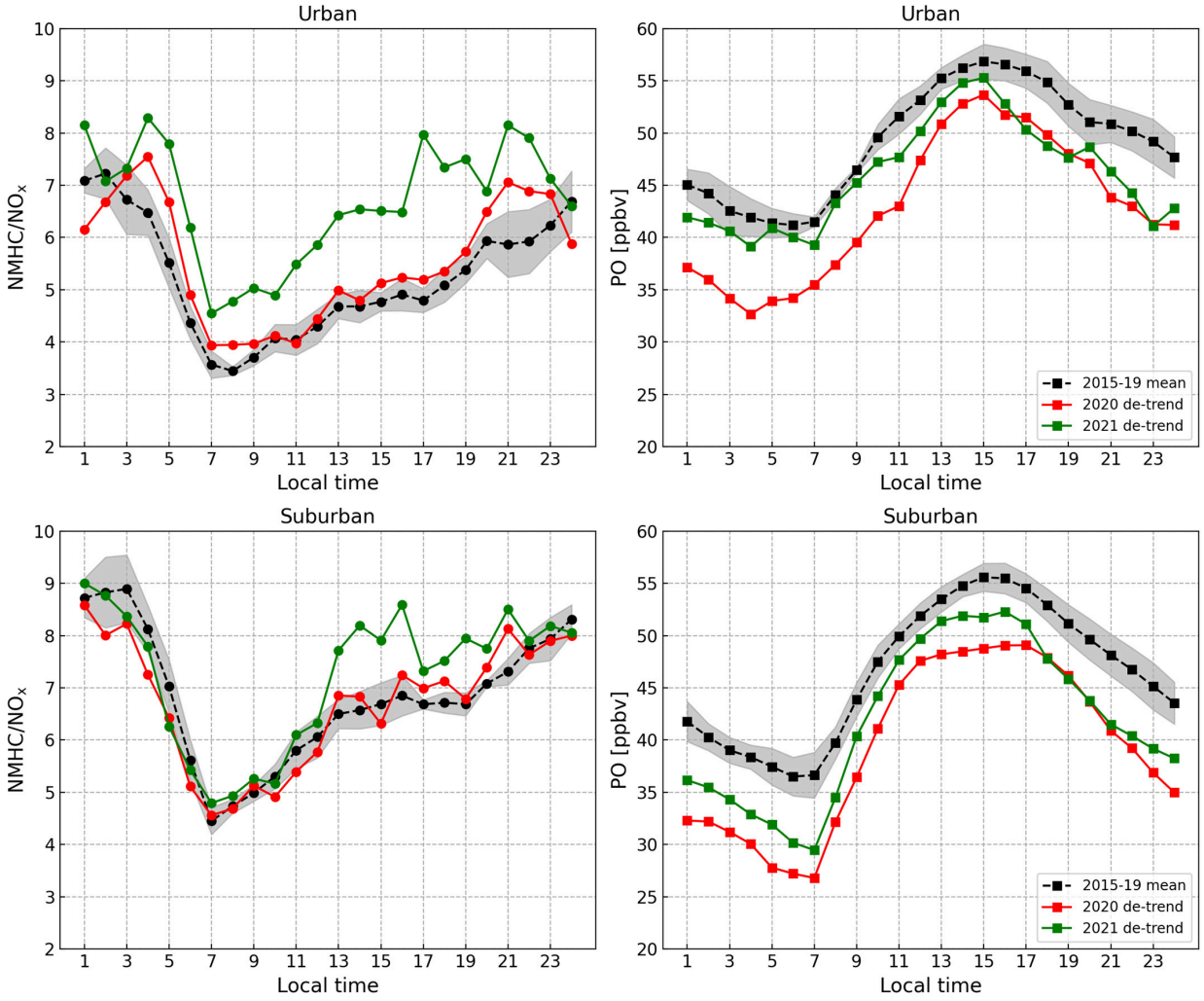

Figure 13. Diurnal variations in NMHC/NO_x (left column) and PO (right column) observed by AEROS in March on weekdays at sites in urban areas (upper row) and suburban areas (lower row).

We quantified baseline O_3 reductions during the COVID-19 pandemic in both urban and suburban areas. Figure 14 shows scatterplots of hourly differences in NO_2 (ΔNO_2) and O_3 (ΔO_3) data between pre- and peri-COVID-19 pandemic periods (i.e., 2020 or 2021 minus 2015–2019), illustrating the interaction between the two species during the pandemic. The orange (blue) dots indicate the AEROS data observed in daytime (nighttime). The blue (red) lines show linear regression fits for negative (positive) ΔNO_2 values. Overall, during nighttime (18:00−6:00; blue circles in Figure 14), ΔNO_2 tended to be near zero or slightly positive while ΔO_3 was relatively lower; during daytime (6:00−18:00; orange circles in Figure 14), ΔNO_2 was lower than at night while ΔO_3 was higher. In this analysis, we attempted to introduce an original two-step fitting method to estimate a baseline O_3 reduction due to the COVID-19 pandemic. First, for cases where ΔNO_2 (x-axis) was positive, we performed a linear regression with a slope fixed at 1 and estimated only the intercept (e.g., red broken lines in Figure 14). Second, using the fitted intercept above, we performed a similar regression for cases where ΔNO_2 was negative, estimating only the slope (e.g., blue broken lines in Figure 14). This method was based on two assumptions: (1) the de-trending method used in this study effectively removes the yearly trend so that the Δ values reflect only the effects of the COVID-19 pandemic, and (2) nighttime NO_2 concentration

increases mainly result from the O_3 + NO reaction. Under this framework, therefore, the intercept (ΔO_3 value when $\Delta NO_2 = 0$) represents the baseline O_3 concentration reductions during the COVID-19 pandemic because ΔO_3 values should converge to 0 if the two assumptions mentioned above are valid and ΔNO_2 equals 0. Using this approach, the baseline O_3 reductions were estimated to range from 2.5 ppbv to 8.5 ppbv depending on the site and year. In the urban area in 2020, variation in NO_2 showed a linear relationship with variations in O_3 concentration across the full range, indicating that NO_2 reductions during the COVID-19 pandemic contributed linearly to slower O_3 formation. In the suburban area in 2020, however, the slopes fitted for negative ΔNO_2 values were steeper than −2.0, which means that NO_2 reductions were associated with an obstruction of O_3 reduction during the COVID-19 pandemic. Although there are many limitations and assumptions in this experimental analytical method, the derived baseline O_3 reductions showed all negative values and were slightly plausible in 2020. At the very least, the same magnitude of the reductions can be seen in both the urban and suburban areas in 2020, suggesting that the O_3 concentration in March of 2020 did not increase due to the weakening of NO titration, as several previous studies have reported [32,43,44].

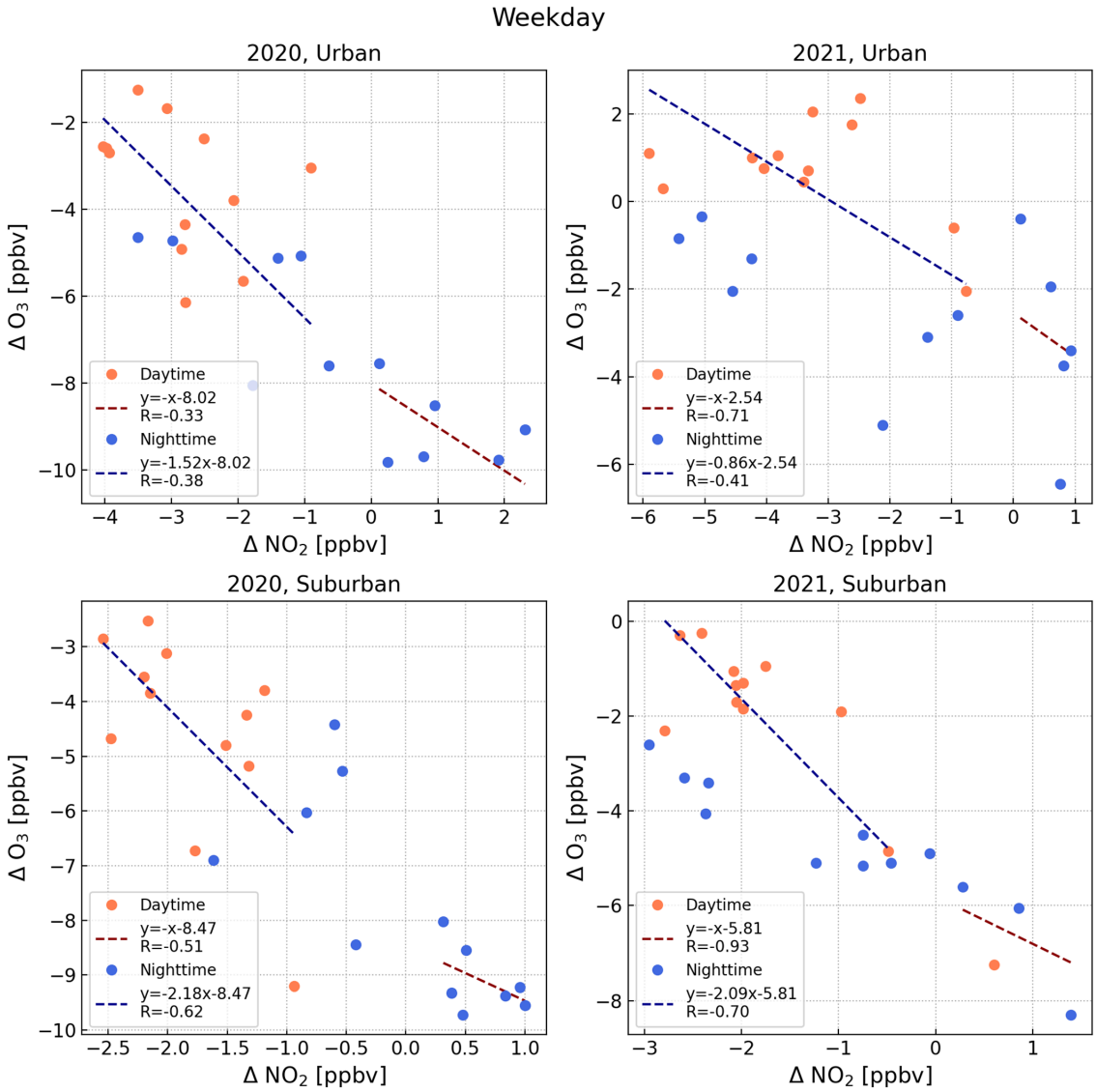

Figure 14. Scatterplots of AEROS ΔNO_2 and ΔO_3 in March (weekdays) for urban and suburban sites, comparing business-as-usual (BAU) conditions with 2020 (**left column**) and 2021 (**right column**). See the text for details of the fitting method and interpretation.

As summarized in Table 2, baseline O_3 reductions were comparable to decreases in PO values, especially in 2020, which indicates that the estimated baseline O_3 reduction was attributable to precursor decreases and advection outside the domain. The PO reduction can explain 78.8–83.5% of the reduction in baseline O_3 in 2020. To quantitatively analyze the contributions of precursor decreases and advection, it may be necessary to further conduct sensitivity tests and simulation analyses using a chemical transfer model, which was not performed in this study. However, the results in this study imply that to decrease local emission of precursors such as NO_2 and NMHCs, it is important to decrease baseline O_3 especially during daytime.

Table 2. Summary of reductions in baseline O_3 and PO and percentages of PO/baseline O_3 in 2020 and 2021.

	Baseline O_3 Reduction [ppbv]	**PO Reduction [ppbv]**	**Percentage Ratio of Baseline O_3 Reduction and PO Reduction (PO/O_3) [%]**
Urban	8.0 (2.5)	6.3 (3.2)	78.8 (128)
Suburban	8.5 (5.8)	7.1 (4.7)	83.5 (81.0)

The values in 2021 are in parentheses.

4. Conclusions

This study examined atmospheric behavior in urbanized cities of Japan during the COVID-19 pandemic to evaluate the effects of reduced human activity on ambient air quality, providing information relevant to air pollution control policies. In Japan, especially in the highly urbanized Kanto region, human mobility decreased by up to 70% due to COVID-19-related movement restrictions. Based on satellite observations of NO_2 VCDs, we estimated 16–38% reductions in tropospheric NO_2 VCD in the Kanto region from March to April in 2020, relative to pre-COVID-19 conditions, which is in good agreement with a previous report [23]. We also analyzed the effect of the COVID-19 pandemic on air quality using ground-based in situ measurements (AEROS), which are widely and densely deployed in Japan, accounting for year-to-year trends of atmospheric species. The results indicated that surface NO_2 concentration decreased by 12–22% in March 2020 and 2021, when marked NO_2 reductions were also seen in the satellite data, compared with mean values for the same months of 2015–2019. These reductions were broadly consistent with the satellite results. In the urban area, surface O_3 concentrations similarly decreased in 2020 by an average of 18.2%, with a maximum reduction of 33.4%, although O_3 concentration levels returned to 2015–2019 levels in 2021. In the suburban area, reductions of comparable magnitude were observed, and the maximum O_3 concentration in 2020 became comparable to that in the urban area. We calculated diurnal variations in the NMHC/NO_x and potential ozone (PO = O_3 + NO_2 − 0.1NO_x) to assess ozone-formation regimes. These analyses indicated that during the COVID-19 pandemic, both urban and suburban areas might remain within the boundary between NMHC- (VOC-) and NO_x-limited regimes at nighttime and VOC-limited during daytime. The NMHC/NO_x during the COVID-19 pandemic was comparable to pre-pandemic values. PO concentrations in 2020 were lower by 6.3 ppbv in the urban area and 7.1 ppbv in the suburban area, respectively, than in 2015–2019. The daytime decreases in NO_2 and NMHC concentrations likely lead to relatively lower O_3 concentrations during daytime and subsequent low levels of O_3 concentration at night, which implies that measures for air pollution control during daytime are likely to be effective for mitigation of the background O_3 concentration level. Analysis of the differences in O_3 and NO_2 between pre- and peri-COVID-19 periods (2015–2019 versus 2020–2021) showed a baseline O_3 reduction of up to 8.5 ppbv, which is

partly explained by PO reduction. Our results showed O_3 reduction under the condition of a NO_2 decrease in urban areas, which may indicate a different situation than previously reported. In this study, meteorological effects on formation and destruction of trace gases were simply considered by including meteorological variables in a linear regression. Future work may consider chemical and meteorological conditions, as well as transport from outside of the domain, e.g., using CTM.

Supplementary Materials: The following supporting information can be downloaded at https://www.mdpi.com/article/10.3390/atmos17050491/s1. Table S1. Summary statistics of the AEROS NO_2 and O_3 concentrations in urban areas. Table S2. Same as S1 but in suburban areas. Table S3. Minimum, maximum and δO_3 (difference between maximum and minimum O_3) values of diurnal O_3 concentrations in urban and suburban areas. Texts in the parentheses in the Min. (Max.) column show the local time the minimum (or maximum) was observed. Figure S1. Box–whisker plots of monthly and diurnal variations in surface NO_2 concentration measured by AEROS in the Kanto region for different methods. Figure S2. Yearly trend of NO_2 and O_3 medians in March during weekdays for urban and suburban areas. Figure S3. Yearly trend of AEROS surface concentrations for NO_2, O_3, NO_x and NMHCs measured in March. Figure S4. Same as Figures 11 and 12 but for NOx and NO. Figure S5. Box-and-whisker plots of the hourly correction factors (δ_{cor}) used for de-trending in this study for NO2, O3 and NMHCs. The bottom and top of the boxes mean 25%ile and 75%ile. The bars in the boxes mean median values. The lower and upper edges of the whiskers represent the minimum and maximum values, except for outliers. The triangles represent mean values. Figure S6. Box–whisker plots of minimum (upper) and maximum (middle) values and differences (δO_3) in O_3 concentrations (bottom) for each year in urban areas. A brown box represents a box–whisker of the mean values in 2015–2019. The titles represent the local time when the values were observed. Note that the maximum values in 2020 and 2021 were observed at 14:00. The means of the boxes and whiskers are the same as those in Figure S5. Figure S7. Same as Figure S6 but for suburban areas.

Author Contributions: Conceptualization, T.F.; methodology, T.F., S.I., H.T., T.S., M.Y. and K.I.; formal analysis, T.F.; writing—original draft preparation, T.F.; writing—review and editing, H.T., T.F., S.I., M.Y. and K.I.; visualization, T.F.; supervision, S.I. and H.T. All authors have read and agreed to the published version of the manuscript.

Funding: This research received no external funding.

Data Availability Statement: The AEROS data are available at https://soramame.env.go.jp/ (accessed on 14 April 2026). The OMI and TROPOMI NO_2 data are both available at the NASA Goddard Earth Sciences Data and Information Services Center (GES DISC) (https://disc.gsfc.nasa.gov/: accessed on 14 April 2026). The COVID-19 Community Mobility Reports produced by Google are available at https://www.google.com/covid19/mobility/ (accessed on 14 April 2026).

Acknowledgments: We are grateful to the Ministry of the Environment, Japan, for providing AEROS data, and to NASA GES DISC for distributing the OMNO2d and TROPOMI_MINDS_NO2 products.

Conflicts of Interest: The authors declare no conflicts of interest.

Abbreviations

The following abbreviations are used in this manuscript:

AEROS	Atmospheric Environmental Regional Observation System
BAU	Business-as-usual
COVID-19	Coronavirus disease in 2019
CTM	Chemical transfer model
GES DISC	Goddard Earth Sciences Data and Information Services Center
GLM	Generalized linear model
GOME	Global Ozone Monitoring Experiment
LST	Local solar time

MAE	Mean absolute error
MEaSUREs	Making Earth System Data Records for Use in Research Environments program
NMHC	Non-methane hydrocarbon
OMI	Ozone Monitoring Instrument
PO	Potential ozone
ppbv	Parts per billion by volume
SCD	Slant column density
SCIAMACHY	SCanning Imaging Absorption SpectroMeter for Atmospheric CHartographY
SoE	State of emergency
TROPOMI	TROPOspheric Monitoring Instrument
TVCD	Tropospheric vertical column density
VCD	Vertical column density
VOC	Volatile organic compound

References

1. Seinfeld, J.H.; Pandis, S.N. *Atmospheric Chemistry and Physics: From Air Pollution to Climate Change*; John Wiley & Sons: Hoboken, NJ, USA, 2016.
2. Mazzuca, G.M.; Ren, X.; Loughner, C.P.; Estes, M.; Crawford, J.H.; Pickering, K.E.; Weinheimer, A.J.; Dickerson, R.R. Ozone Production and Its Sensitivity to NO_x and VOCs: Results from the DISCOVER-AQ Field Experiment, Houston 2013. *Atmos. Chem. Phys.* **2016**, *16*, 14463–14474. [CrossRef]
3. Ren, X.; Van Duin, D.; Cazorla, M.; Chen, S.; Mao, J.; Zhang, L.; Brune, W.H.; Flynn, J.H.; Grossberg, N.; Lefer, B.L.; et al. Atmospheric Oxidation Chemistry and Ozone Production: Results from SHARP 2009 in Houston, Texas. *JGR Atmos.* **2013**, *118*, 5770–5780. [CrossRef]
4. Sadanaga, Y.; Sengen, M.; Takenaka, N.; Bandow, H. Analyses of the Ozone Weekend Effect in Tokyo, Japan: Regime of Oxidant (O_3 + NO_2) Production. *Aerosol Air Qual. Res.* **2012**, *12*, 161–168. [CrossRef]
5. Irie, H.; Yonekawa, D.; Damiani, A.; Hoque, H.M.S.; Sudo, K.; Itahashi, S. Continuous Multi-Component MAX-DOAS Observations for the Planetary Boundary Layer Ozone Variation Analysis at Chiba and Tsukuba, Japan, from 2013 to 2019. *Prog. Earth Planet Sci.* **2021**, *8*, 31. [CrossRef]
6. Itahashi, S.; Irie, H.; Shimadera, H.; Chatani, S. Fifteen-Year Trends (2005–2019) in the Satellite-Derived Ozone-Sensitive Regime in East Asia: A Gradual Shift from VOC-Sensitive to NO_x-Sensitive. *Remote Sens.* **2022**, *14*, 4512. [CrossRef]
7. Jin, X.; Yang, Y.; Gonzalez Abad, G.; Nowlan, C.; Liu, X. Observing the Diurnal Variations of Ozone-NO_x-VOC Chemistry Over the U.S. From the Geostationary TEMPO Instrument. *Geophys. Res. Lett.* **2025**, *52*, e2025GL116394. [CrossRef]
8. Murphy, J.G.; Day, D.A.; Cleary, P.A.; Wooldridge, P.J.; Millet, D.B.; Goldstein, A.H.; Cohen, R.C. The Weekend Effect within and Downwind of Sacramento—Part 1: Observations of Ozone, Nitrogen Oxides, and VOC Reactivity. *Atmos. Chem. Phys.* **2007**, *7*, 5327–5339. [CrossRef]
9. Sadanaga, Y.; Shibata, S.; Hamana, M.; Takenaka, N.; Bandow, H. Weekday/Weekend Difference of Ozone and Its Precursors in Urban Areas of Japan, Focusing on Nitrogen Oxides and Hydrocarbons. *Atmos. Environ.* **2008**, *42*, 4708–4723. [CrossRef]
10. Burrows, J.P.; Weber, M.; Buchwitz, M.; Rozanov, V.; Ladstätter-Weißenmayer, A.; Richter, A.; DeBeek, R.; Hoogen, R.; Bramstedt, K.; Eichmann, K.-U.; et al. The Global Ozone Monitoring Experiment (GOME): Mission Concept and First Scientific Results. *J. Atmos. Sci.* **1999**, *56*, 151–175. [CrossRef]
11. Bovensmann, H.; Burrows, J.P.; Buchwitz, M.; Frerick, J.; Noël, S.; Rozanov, V.V.; Chance, K.V.; Goede, A.P.H. SCIAMACHY: Mission Objectives and Measurement Modes. *J. Atmos. Sci.* **1999**, *56*, 127–150. [CrossRef]
12. Levelt, P.F.; Hilsenrath, E.; Leppelmeier, G.W.; Van Den Oord, G.H.; Bhartia, P.K.; Tamminen, J.; De Haan, J.F.; Veefkind, J.P. Science Objectives of the Ozone Monitoring Instrument. *IEEE Trans. Geosci. Remote Sens.* **2006**, *44*, 1199–1208. [CrossRef]
13. Veefkind, J.P.; Aben, I.; McMullan, K.; Förster, H.; De Vries, J.; Otter, G.; Claas, J.; Eskes, H.J.; De Haan, J.F.; Kleipool, Q. TROPOMI on the ESA Sentinel-5 Precursor: A GMES Mission for Global Observations of the Atmospheric Composition for Climate, Air Quality and Ozone Layer Applications. *Remote Sens. Environ.* **2012**, *120*, 70–83. [CrossRef]
14. Azuma, K.; Kagi, N.; Kim, H.; Hayashi, M. Impact of Climate and Ambient Air Pollution on the Epidemic Growth during COVID-19 Outbreak in Japan. *Environ. Res.* **2020**, *190*, 110042. [CrossRef] [PubMed]
15. Liu, F.; Page, A.; Strode, S.A.; Yoshida, Y.; Choi, S.; Zheng, B.; Lamsal, L.N.; Li, C.; Krotkov, N.A.; Eskes, H.; et al. Abrupt Decline in Tropospheric Nitrogen Dioxide over China after the Outbreak of COVID-19. *Sci. Adv.* **2020**, *6*, eabc2992. [CrossRef]
16. Petetin, H.; Bowdalo, D.; Soret, A.; Guevara, M.; Jorba, O.; Serradell, K.; Pérez García-Pando, C. Meteorology-Normalized Impact of the COVID-19 Lockdown upon NO_2 Pollution in Spain. *Atmos. Chem. Phys.* **2020**, *20*, 11119–11141. [CrossRef]

17. Albanai, J.A.; Shehab, M.; Vatresia, A.; Jasim, M.; Al-Dashti, H.; Yassin, M.F. Impact of Coronavirus Disease (COVID-19) on Gaseous Pollutants and Particulate Matter in a Hot Arid Climate. *Kuwait J. Sci.* **2025**, *52*, 100351. [CrossRef]
18. Fitria, A.N.; Supriyadi, S.; Al-Irsyad, M.; Hapsari, A. Impact of Large-Scale Social Restrictions on Air Quality (NO_2, CO, O_3) during COVID-19: Surabaya Case Study, Indonesia. *Public Health Occup. Saf. J.* **2025**, *1*, 27–39. [CrossRef]
19. Wang, D.; Pu, D.; De Smedt, I.; Zhu, L.; Yang, X.; Sun, W.; Xia, H.; Song, Z.; Li, X.; Li, J.; et al. Evolution of Global O_3-NO_x-VOCs Sensitivity before and after the COVID-19 from the Ratio of Formaldehyde to NO_2 from Satellite Observations. *J. Environ. Sci.* **2025**, *156*, 102–113. [CrossRef]
20. de Souza, A.; Nofiu Idowu, B.; Francisco de Oliveira Júnior, J.; Gautam, S. Adjustment of Statistical Distributions to O_3 and NO_2 Concentrations in the Pre-COVID-19 Periods and during the Pandemic in Campo Grande, MS, Brazil. *J. Environ. Eng. Sci.* **2025**, *20*, 295–308. [CrossRef]
21. Miyazaki, K.; Bowman, K.; Sekiya, T.; Takigawa, M.; Neu, J.L.; Sudo, K.; Osterman, G.; Eskes, H. Global Tropospheric Ozone Responses to Reduced NOx Emissions Linked to the COVID-19 Worldwide Lockdowns. *Sci. Adv.* **2021**, *7*, eabf7460. [CrossRef]
22. Shi, Z.; Song, C.; Liu, B.; Lu, G.; Xu, J.; Van Vu, T.; Elliott, R.J.R.; Li, W.; Bloss, W.J.; Harrison, R.M. Abrupt but Smaller than Expected Changes in Surface Air Quality Attributable to COVID-19 Lockdowns. *Sci. Adv.* **2021**, *7*, eabd6696. [CrossRef]
23. Damiani, A.; Irie, H.; Belikov, D.A.; Kaizuka, S.; Hoque, H.M.S.; Cordero, R.R. Peculiar COVID-19 Effects in the Greater Tokyo Area Revealed by Spatiotemporal Variabilities of Tropospheric Gases and Light-Absorbing Aerosols. *Atmos. Chem. Phys.* **2022**, *22*, 12705–12726. [CrossRef]
24. Phan, A.; Fukui, H. Unusual Response of O_3 and CH_4 to NO_2 Emissions Reduction in Japan during the COVID-19 Pandemic. *Int. J. Digit. Earth* **2024**, *17*, 2297844. [CrossRef]
25. COVID-19 Community Mobility Report. Available online: https://www.google.com/covid19/mobility?hl=ja (accessed on 26 April 2026).
26. Hilboll, A.; Richter, A.; Burrows, J.P. Long-Term Changes of Tropospheric NO_2 over Megacities Derived from Multiple Satellite Instruments. *Atmos. Chem. Phys.* **2013**, *13*, 4145–4169. [CrossRef]
27. Cooper, M.J.; Martin, R.V.; Hammer, M.S.; Levelt, P.F.; Veefkind, P.; Lamsal, L.N.; Krotkov, N.A.; Brook, J.R.; McLinden, C.A. Global Fine-Scale Changes in Ambient NO_2 during COVID-19 Lockdowns. *Nature* **2022**, *601*, 380–387. [CrossRef] [PubMed]
28. Ito, A.; Wakamatsu, S.; Morikawa, T.; Kobayashi, S. 30 Years of Air Quality Trends in Japan. *Atmosphere* **2021**, *12*, 1072. [CrossRef]
29. Han, S.; Bian, H.; Feng, Y.; Liu, A.; Li, X.; Zeng, F.; Zhang, X. Analysis of the Relationship between O_3, NO and NO_2 in Tianjin, China. *Aerosol Air Qual. Res.* **2011**, *11*, 128–139. [CrossRef]
30. Akimoto, H.; Mori, Y.; Sasaki, K.; Nakanishi, H.; Ohizumi, T.; Itano, Y. Analysis of Monitoring Data of Ground-Level Ozone in Japan for Long-Term Trend during 1990–2010: Causes of Temporal and Spatial Variation. *Atmos. Environ.* **2015**, *102*, 302–310. [CrossRef]
31. Itahashi, S.; Shimadera, H.; Irie, H.; Kitayama, K.; Chatani, S. Changes in Ambient Ozone Concentrations from Urban to Remote Areas in Japan during the COVID-19 Pandemic Period in April and May, 2020. *Prog. Earth Planet Sci.* **2026**, *13*, 5. [CrossRef]
32. Gkatzelis, G.I.; Gilman, J.B.; Brown, S.S.; Eskes, H.; Gomes, A.R.; Lange, A.C.; McDonald, B.C.; Peischl, J.; Petzold, A.; Thompson, C.R.; et al. The Global Impacts of COVID-19 Lockdowns on Urban Air Pollution: A Critical Review and Recommendations. *Elem. Sci. Anthr.* **2021**, *9*, 00176. [CrossRef]
33. Heald, C.L.; Kroll, J.H.; Murphy, J.G.; Farmer, D.K.; Fry, J.L. Atmospheric Chemistry Insights from the Global COVID-19 Pandemic: A Review. *Environ. Sci. Technol.* **2026**, *60*, 10393–10404. [CrossRef] [PubMed]
34. Itano, Y.; Bandow, H.; Takenaka, N.; Saitoh, Y.; Asayama, A.; Fukuyama, J. Impact of NO_x Reduction on Long-Term Ozone Trends in an Urban Atmosphere. *Sci. Total Environ.* **2007**, *379*, 46–55. [CrossRef] [PubMed]
35. Hata, H.; Mizushima, N.; Ihara, T. Impact of Introducing Electric Vehicles on Ground-Level O_3 and $PM_{2.5}$ in the Greater Tokyo Area: Yearly Trends and the Importance of Changes in the Urban Heat Island Effect. *Atmos. Chem. Phys.* **2025**, *25*, 1037–1061. [CrossRef]
36. Liu, C.; Zhang, L.; Wen, Y.; Shi, K. Sensitivity Analysis of O_3 Formation to Its Precursors-Multifractal Approach. *Atmos. Environ.* **2021**, *251*, 118275. [CrossRef]
37. Sharma, A.; Sharma, S.K.; Mandal, T.K. Ozone Sensitivity Factor: NO_X or NMHCs? A Case Study over an Urban Site in Delhi, India. *Urban Clim.* **2021**, *39*, 100980. [CrossRef]
38. Carslaw, D.C.; Rhys-Tyler, G. New Insights from Comprehensive On-Road Measurements of NO_x, NO_2 and NH_3 from Vehicle Emission Remote Sensing in London, UK. *Atmos. Environ.* **2013**, *81*, 339–347. [CrossRef]
39. Matthaios, V.N.; Kramer, L.J.; Sommariva, R.; Pope, F.D.; Bloss, W.J. Investigation of Vehicle Cold Start Primary NO_2 Emissions Inferred from Ambient Monitoring Data in the UK and Their Implications for Urban Air Quality. *Atmos. Environ.* **2019**, *199*, 402–414. [CrossRef]
40. Carslaw, D.C.; Farren, N.J.; Vaughan, A.R.; Drysdale, W.S.; Young, S.; Lee, J.D. The Diminishing Importance of Nitrogen Dioxide Emissions from Road Vehicle Exhaust. *Atmos. Environ. X* **2019**, *1*, 100002. [CrossRef]

41. Brimblecombe, P.; Chu, M.; Liu, C.-H.; Fu, Y.; Wei, P.; Ning, Z. Roadside NO_2/NO_x and Primary NO_2 from Individual Vehicles. *Atmos. Environ.* **2023**, *295*, 119562. [CrossRef]
42. Minoura, H.; Ito, A. Observation of the Primary NO_2 and NO Oxidation near the Trunk Road in Tokyo. *Atmos. Environ.* **2010**, *44*, 23–29. [CrossRef]
43. Sicard, P.; De Marco, A.; Agathokleous, E.; Feng, Z.; Xu, X.; Paoletti, E.; Rodriguez, J.J.D.; Calatayud, V. Amplified Ozone Pollution in Cities during the COVID-19 Lockdown. *Sci. Total Environ.* **2020**, *735*, 139542. [CrossRef]
44. Venter, Z.S.; Aunan, K.; Chowdhury, S.; Lelieveld, J. COVID-19 Lockdowns Cause Global Air Pollution Declines. *Proc. Natl. Acad. Sci. USA* **2020**, *117*, 18984–18990. [CrossRef]